Redox Biology 37 (2020) 101723

Contents lists available at ScienceDirect

Redox Biology

journal homepage: www.elsevier.com/locate/redox

Research Paper

Elevated 4-hydroxynonenal induces hyperglycaemia via Aldh3a1 loss in zebrafish and associates with diabetes progression in humans

Bowen Lou [a,b], Mike Boger [a], Katrin Bennewitz [a], Carsten Sticht [c], Stefan Kopf [d,e], Jakob Morgenstern [d,e], Thomas Fleming [d,e], Rüdiger Hell [f], Zuyi Yuan [b], Peter Paul Nawroth [d,e,g], Jens Kroll [a,*]

[a] Department of Vascular Biology and Tumor Angiogenesis, European Center for Angioscience (ECAS), Medical Faculty Mannheim, Heidelberg University, Mannheim, Germany
[b] Cardiovascular Department, The First Affiliated Hospital of Xi'an Jiaotong University, Xi'an, 710048, China
[c] Center for Medical Research (ZMF), Medical Faculty Mannheim, Heidelberg University, Mannheim, Germany
[d] Department of Internal Medicine I and Clinical Chemistry, Heidelberg University Hospital, Heidelberg, Germany
[e] German Center for Diabetes Research (DZD), Neuherberg, Germany
[f] Metabolomics Core Technology Platform, Centre for Organismal Studies, Heidelberg University, Heidelberg, Germany
[g] Joint Heidelberg-IDC Translational Diabetes Program, Helmholtz-Zentrum, München, Heidelberg, Germany

ARTICLE INFO

Keywords:
Aldh3a1
Reactive carbonyl species
4-hydroxynonenal
Glucose homeostasis
Diabetes

ABSTRACT

Increased methylglyoxal (MG) formation is associated with diabetes and its complications. In zebrafish, knockout of the main MG detoxifying system Glyoxalase 1, led to limited MG elevation but significantly elevated aldehyde dehydrogenases (ALDH) activity and *aldh3a1* expression, suggesting the compensatory role of Aldh3a1 in diabetes. To evaluate the function of Aldh3a1 in glucose homeostasis and diabetes, *aldh3a1*$^{-/-}$ zebrafish mutants were generated using CRISPR-Cas9. Vasculature and pancreas morphology were analysed by zebrafish transgenic reporter lines. Corresponding reactive carbonyl species (RCS), glucose, transcriptome and metabolomics screenings were performed and ALDH activity was measured for further verification. *Aldh3a1*$^{-/-}$ zebrafish larvae displayed retinal vasodilatory alterations, impaired glucose homeostasis, which can be aggravated via *pdx1* silencing induced hyperglycaemia. Unexpectedly, MG was not altered, but 4-hydroxynonenal (4-HNE), another prominent lipid peroxidation RCS exhibited high affinity with Aldh3a1, was increased in *aldh3a1* mutants. 4-HNE was responsible for the retinal phenotype via pancreas disruption induced hyperglycaemia and can be rescued via L-Carnosine treatment. Furthermore, in type 2 diabetic patients, serum 4-HNE was increased and correlated with disease progression. Thus, our data suggest impaired 4-HNE detoxification and elevated 4-HNE concentration as biomarkers but also the possible inducers for diabetes, from genetic susceptibility to the pathological progression.

1. Introduction

The prevalence of diabetes in people aged 20–79 years is rising rapidly, from 151 million (4.6% of the global population) in 2000 to 463 million (9.3%) in 2019 and is expected to 700 million (10.9%) in 2045 [1]. Diabetic patients have an increased risk of developing microvascular and macrovascular complications, which can cause blindness, kidney failure, and lower limb amputation [2]. For instance, diabetic retinopathy (DR) is a common microvascular complication of diabetes and the leading cause of vision loss in working-age people [3]. Since patients with severe degrees of DR suffer weakened life quality by decreased physical, emotional and social well-being and increased health-care resources [4], early diagnose and timely treatment of DR is essential for preventing sight impairment and blindness.

As a reactive carbonyl species (RCS), methylglyoxal (MG) is the main precursor of advanced glycation end products (AGEs) [5]. MG is elevated in the plasma and tissue of diabetic patients [6,7] and AGEs are strongly linked to the development of microvascular complications [8,9]. Apart from glyoxalase, the central MG detoxification system [6], MG can also be detoxified by aldo-keto-reductase and aldehyde dehydrogenase (ALDH) [10,11]. A recent study showed knockout of glyoxalase 1

* Corresponding author. European Center for Angioscience (ECAS), Department of Vascular Biology and Tumor Angiogenesis, Medical Faculty Mannheim, Heidelberg University, Ludolf Krehl Str.13–17, 68167, Mannheim, Germany.
E-mail address: jens.kroll@medma.uni-heidelberg.de (J. Kroll).

https://doi.org/10.1016/j.redox.2020.101723
Received 30 July 2020; Received in revised form 31 August 2020; Accepted 11 September 2020
Available online 16 September 2020

Abbreviations

4-HNE	4-hydroxynonenal
AGEs	advanced glycation end products
ALDH	aldehyde dehydrogenase
Aldh3a1	aldehyde dehydrogenase 3 families, member A1
DR	diabetic retinopathy
IR	insulin resistance
MG	methylglyoxal
Pdx1	pancreatic and duodenal homeobox 1
RCS	reactive carbonyl species
ROS	reactive oxygen species
T2DM	type 2 diabetes mellitus

(Glo1) only led to a 1.5-fold MG elevation in zebrafish [12]. Whereas a two-fold increase in ALDH activity and significantly raised *aldh3a1* expression were observed in the *glo1* mutants, suggesting Aldh3a1 as an alternative protein for the detoxification of corresponding RCS [12].

In addition to MG, Aldehyde dehydrogenase has a board spectrum of substrates of RCS such as acetaldehyde and 4-hydroxynonenal (4-HNE) [13]. As the most prominent lipid peroxidation specific aldehydes, 4-HNE has drawn significant attention during the last 40 years [14], leading to several damaging effects such as apoptosis, mitochondrial dysfunction, inflammation and proteasome dysfunction in pathological condition [15]. Due to the high reactive property, 4-HNE is associated with the progression of several diseases, including but not limited to, Alzheimer's disease (AD), Parkinson's disease (PD), heart disease, atherosclerosis, cancer and diabetes [16–20].

The role of 4-HNE in diabetes is not well understood and preliminary data also suggest concentration-dependent effects. Below the cytotoxic amount, 4-HNE reacts to high glucose by active peroxisome proliferator-activated receptor δ (PPARδ) complexes and ultimately increase the secretion of insulin in INS-1E beta cells [21]. When the neutralization capacity of 4-HNE is exceeded, it modifies macromolecules structure, conformation and function, accompanied by AGEs and advanced lipoxidation end products (ALEs)' elevation, resulting in β cell dysfunction [22]. 4-HNE exhibits strongly correlation with diabetic nephropathy [23], neuropathy [24] and retinopathy [25]. Yet, appropriate animal models for an endogenous 4-HNE increase are missing to analyse its damaging mechanisms in vivo.

Aldehyde dehydrogenase 3 families, member A1 (Aldh3a1) is a metabolic enzyme that oxidizes mainly toxic lipid peroxidation aldehydes to their corresponding carboxylic acids [26]. Several studies have proven a high ALDH3A1 affinity for 4-HNE but low ability to detoxify malondialdehyde (MDA), in supporting its multifaceted function [27–29]. However, it remained unclear if a permanent knockout of Aldh3a1 causes increased 4-HNE concentration and results in diabetes and organ damage in the end.

Therefore, the study aimed to evaluate the internal level of RCS and consequent effects of Aldh3a1 knockout on glucose metabolism and the retinal vascular system in zebrafish, while also to investigate the clinical relevance of 4-HNE in the sera of diabetic patients. Our data suggest impaired 4-HNE detoxification and elevated 4-HNE concentration as biomarkers but also the possible inducers for diabetes, from genetic susceptibility to the pathological progression.

2. Results

2.1. Sequence alignment of ALDH3A1 among different species and analysis of the aldh3a1 mRNA expression in zebrafish

ALDH3A1 enzyme system exists in human, mouse and zebrafish [30,31], but the similarity of the enzyme protein in the different species has not been described yet. At first, we aligned the amino acid sequence and the alignment showed zebrafish Aldh3a1 shares 61.6% similarity of protein with human ALDH3A1 and 57.6% with mouse; as an enzyme-encoding gene, the active sites: cysteine and glutamic acid are the same in these three species (Fig. 1A). Then, RT-qPCR was performed for a better understanding of the potential expression differences of *aldh3a1* mRNA level in zebrafish regarding the development and organ distribution. Results showed an increased trend of *aldh3a1* mRNA as the larva developed by around 3-fold elevation at 96 hours after post fertilization (hpf) than 24 hpf. While in adult fish, brain and eye were the most expressed organs, with 11- and 7-fold significant elevation compared to heart (Fig. 1B). Altogether, the data have identified the existence of *aldh3a1* in zebrafish larvae and different adult organs, and the possibility for studying ALDH3A1 enzyme system by using zebrafish as a model.

2.2. Generation of Aldh3a1 knockout in zebrafish

Since Aldh3a1 knockout zebrafish model does not exist thus far and to explore the function of Aldh3a1 in zebrafish and diabetes, *aldh3a1*$^{-/-}$ zebrafish were generated by CRISPR-Cas9 technology [32]. We designed a CRISPR-guideRNA (gRNA) targeting exon 2 of *aldh3a1* (Fig. 2A) and injected the *aldh3a1* gRNA with Cas9 mRNA in the cell of zebrafish one-cell stage embryos. After crossing the F0-positive mosaic mutants with wild type line, we identified different mutations in *aldh3a1* and an 11 bases insertion (Fig. 2A) was selected as frameshift mutation for further breeding and experiments, which can be distinguished via genotyping-PCR (Fig. 2B) and lead to the formation of a stop-codon afterwards (Fig. 2C). The gross morphology showed no difference between homozygous and wild type zebrafish larvae at 96 hpf (Fig. 2D). Besides, the fish number was counted by genotype during the first generation of F2. The number of wild type, heterogynous and homozygous adult fish at four months old were 14, 27 and 12 respectively, which was in line with *the Mendelian Inheritance* [33] (Fig. 2E), indicating no survival adversity in *aldh3a1*$^{-/-}$ mutants. To evaluate whether the 11 bases insertion in *aldh3a1* mutants causes the non-functional Aldh3a1 protein after translation, total ALDH activity was measured by using acetaldehyde as substrate and *aldh3a1* mutants displayed 30% significant reduction (Fig. 2F). All the above have proven the successful generation of Aldh3a1 knockout mutants.

2.3. Vascular alterations were enhanced in aldh3a1$^{-/-}$ Tg (fli1:EGFP) zebrafish larvae by endogenous pdx1 expression silencing

Our previous study has confirmed that high tissue glucose induces several malformed and uncoordinated blood vessel structures in zebrafish larvae [34]. To investigate vascular developmental effects potentially caused by Aldh3a1 knockout and under hyperglycaemic condition, we established an *aldh3a1* mutant line carrying the *Tg(fli1:EGFP)* zebrafish reporter to perform this experiment. In normal condition, there was no difference in hyperbranches but a slightly increased sign in abnormal intersegmental vessels (ISVs) between *aldh3a1*$^{+/+}$ and *aldh3a1*$^{-/-}$ zebrafish larvae at 96 hpf (Fig. 3). Since pancreatic and duodenal homeobox 1 (Pdx1) is a necessary transcription factor for pancreatic development, including β cell maturation and duodenal differentiation [35], transient silencing its expression by *pdx1* morpholino injection was used to mediate hyperglycaemia and mimic the diabetic condition. While in morpholino mediated *pdx1* silencing, *aldh3a1*$^{-/-}$ larvae displayed enhanced vascular alterations with both raised numbers of hyperbranches and abnormal ISVs compared to *aldh3a1*$^{+/+}$ larvae at 96 hpf (Fig. 3).

The dilation and weakened constrictive autoregulation of retinal vessels are recognized as an early sign of DR [36]. For understanding the short-term influence of Aldh3a1 knockout and hyperglycaemia on the retinal microvasculature, we analysed the retinal hyaloid network in *Tg (fli1: EGFP)* zebrafish larvae at 120 hpf. *Aldh3a1*$^{-/-}$ larvae exhibited

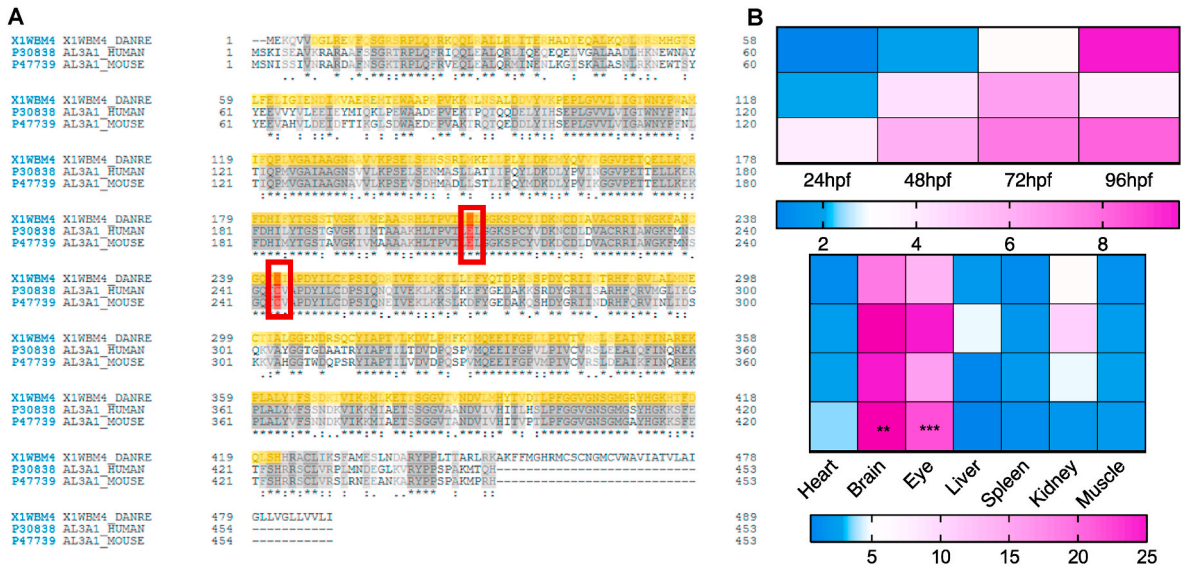

Fig. 1. Sequence alignment of Aldh3a1 across different species and expression of *aldh3a1* mRNA in zebrafish.
(A). Amino acid alignment showed a high similarity and same active sites (red frame) between different species: First line, zebrafish Aldh3a1; Second line, human ALDH3A1; Third line, mouse ALDH3A1. (B). Heatmap of *aldh3a1* mRNA expression in wild type zebrafish showed an increasing trend from 24 hpf to 96 hpf in larvae, and brain and eye were the most expressed adult organs. The higher and lower expression is displayed in pink and blue, respectively. Expression of genes was determined by RT-qPCR and normalized to *b2m*. The average values of 24 hpf wild type larvae and heart (adult organs) were standardized to 1; Larvae: n = 3 clutches with 30 larvae, adult organs: n = 4 with one organ per sample. For statistical analysis one-way ANOVA followed by Sidak's multiple comparison test was applied, **p < 0.01, ***p < 0.001. RT-qPCR, real-time quantitative polymerase chain reaction; hpf, hours after post fertilization; *b2m*, *β2 microglobulin*. (For interpretation of the references to colour in this figure legend, the reader is referred to the Web version of this article.)

widen inner optic circle (IOC) branches, quantified by increased diameters, but no change in sprouts compared to *aldh3a1*$^{+/+}$ (Fig. 4), which implies the early impairment of contraction function in the retinal vessels of *aldh3a1* mutants. Morpholino mediated *pdx1* silencing led to angiogenic retinal vascular alterations, with increased IOC branch diameters and the number of sprouts in *aldh3a1*$^{-/-}$ larvae (Fig. 4). Altogether, these results indicate the moderate vascular alterations after Aldh3a1 loss, which can be enhanced under the hyperglycaemic condition in zebrafish larvae.

2.4. ALDH inhibition, aldh3a1 transient silencing and permanent knockout disrupted the primary endocrine pancreas in zebrafish larvae

Since *aldh3a1* mutants carrying pancreas transgenic reporter haven't been generated yet, for Aldh3a1 functional exploration in the primary pancreas and its interaction with Pdx1, ALDH activity inhibition and *aldh3a1* silencing strategies are essential. Two common ALDH inhibitors, gossypol and N,N-diethylaminobenzaldehyde (DEAB) were selected for performing incubation assays. In addition, to reduce *aldh3a1* expression in zebrafish transiently by the antisense approach, two morpholinos, SB-*aldh3a1*-Mo#1 and SB-*aldh3a1*-Mo#2, were designed and targeted intron3-exon4 and exon4-intron4 junction of *aldh3a1-201* respectively (Fig S1A). The efficiency of morpholino was validated by RT-PCR (Fig S1B) and microscopic images showed normal gross morphology after injection indicating the *aldh3a1* morpholinos do not cause other off-target or toxic effects in extra (Fig S1C).

Since Hb9 (Mnx) is involved in spinal cord motor neuron cell fate specification and pancreatic β cell differentiation [37], we first analysed the primary pancreatic area size by using *Tg(hb9:GFP)* transgenic reporter line (also known as *Tg[mnx1:GFP]*). DEAB treatment and *aldh3a1* silencing mediated by both morpholinos result in the disruption of the primary pancreas, quantified by reduced dimensions in zebrafish larvae at 72 hpf (Fig. 5 A–B). Then β cell mass size analyses were carried out by using *Tg(ins:nfsB-mCherry)* transgenic reporter line, which provides not only a suitable model for β cell regeneration but also an alternative strategy to manipulate cell interactions during early pancreas up-growth [38]. After the quantification, the early β cell mass showed significantly decreased size with SB-*aldh3a1*-Mo#2 injection and DEAB treatment, and a descendant trend with SB-*aldh3a1*-Mo#1 injection in zebrafish larvae at 72 hpf (Fig. 5 A and C). These results demonstrate the disrupted primary morphology mediated by *aldh3a1* silencing and ALDH inhibition in zebrafish.

The pancreas plays a fundamental role in insulin secretion and hereby regulates glucose [39]. To clarify the consequence of pancreatic dysplasia caused by the lack of Aldh3a1, *preproinsulin (ins)*, *preproinsulin b (insb)* and *pdx1* mRNA expression were determined via a RT-qPCR based approach. We found *ins* and *pdx1* were significantly reduced in ALDH activity inhibited, both *aldh3a1* silencing and knockout larvae at 48 hpf. *Insb,* another insulin-encoding gene involved in glucose homeostasis regulation while also acted as a pro-growth, survival, and neurotrophic factor during development [40], was unaltered, indicating *insb* cannot compensate for the decreased insulin secretion (Fig. 5 D-E, Fig S2). Besides, in *aldh3a1*$^{-/-}$ larvae, pancreas development-related genes, *ISL LIM homeobox 1 (isl 1)* and *ISL LIM homeobox 2a (isl2a)* mRNA showed decreased trends while *ISL LIM homeobox 2b (isl2b)* mRNA reduced strongly compared to *aldh3a1*$^{+/+}$ larvae at 48 hpf (Fig S3).

Furthermore, to understand how the impaired pancreas reflects at the transcriptome level, we performed full genome RNA-Seq between *aldh3a1*$^{+/+}$ and *aldh3a1*$^{-/-}$ larvae at 48 hpf (Fig. 6A). An overview of RNA-Seq, including quality control, principal component analysis (PCA), volcano plots of regulated genes and Top 20 KEGG pathway analysis showed comparable properties between aldh3a1 mutants and wild type (Fig S4 A-D). In line with decreased ins expression result, we found the insulin signalling pathway was reduced significantly via KEGG analysis (normalized enrichment score, −1.72; adjust p = 0.003; Fig. 6 B–C and Table S6). Interestingly, endocrine pancreas but not exocrine pancreas development pathway was significantly down-regulated in aldh3a1 mutants (Fig. 6 C–F). Taken together, these results further suggest Aldh3a1 as an important regulator in the development, morphology and insulin secretion function of primary pancreas.

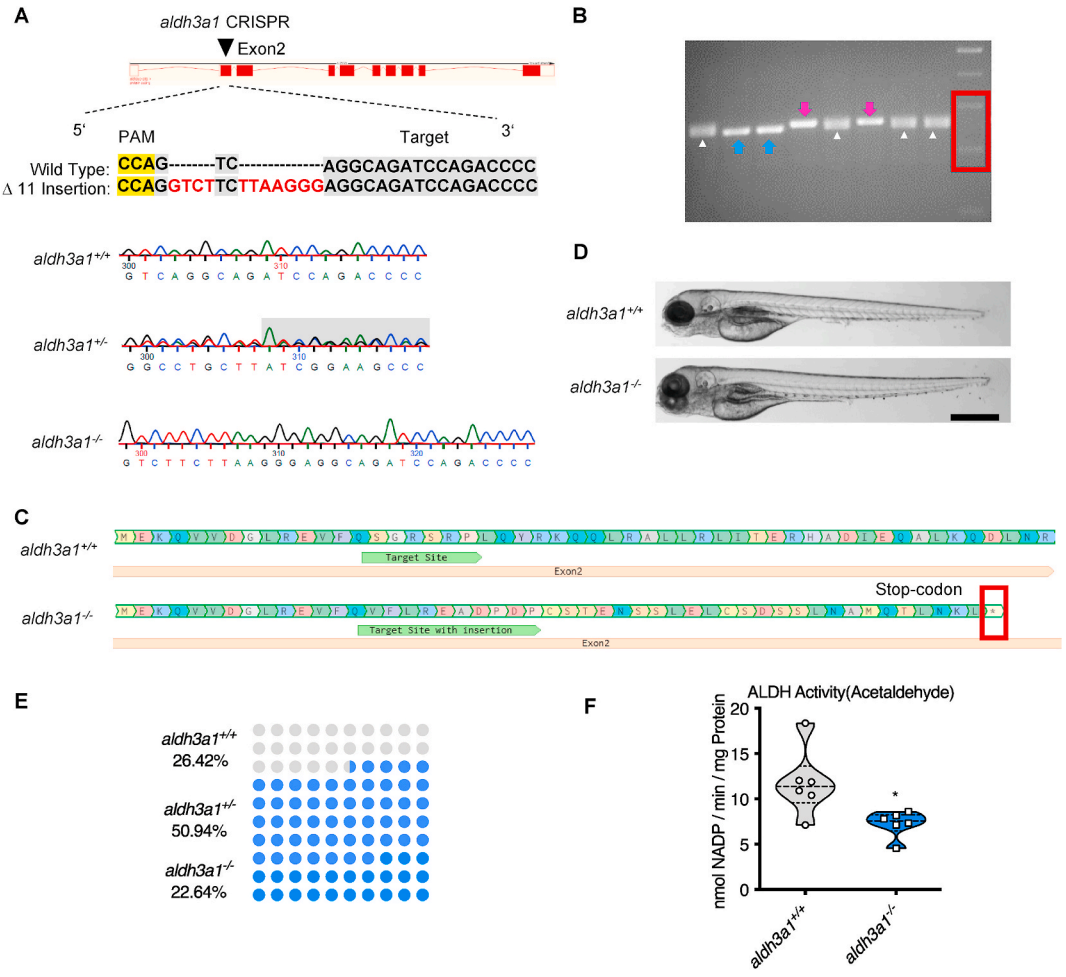

Fig. 2. Generation of Aldh3a1 knockout zebrafish by using CRISPR-Cas9 technology.
(A). *Aldh3a1*-CRISPR-target site was designed in exon2 of *aldh3a1* and CRISPR/Cas9-induced insertions of 11 nucleotides was selected for further investigation. Genotype was analysed and chromatogram showed *aldh3a1* wild type, heterozygous, and homozygous sequencing results. (B). Genotyping-PCR gel showed the distinguishable bands of *aldh3a1* wild type, homozygous and heterozygous zebrafish mutant line. The blue arrows, purple arrows and white deltas indicate the genotyping-PCR products from *aldh3a1* wild type, homozygous and heterozygous zebrafish, respectively. The red frame indicates the marker, lower band is 200 bp and upper band is 300 bp. PCR product size: wildtype, 255 bp; homozygous, 266 bp. (C). Amino acid sequence showed a stop-codon in exon2 of $aldh3a1^{-/-}$. (D). Microscopic images showed normal gross morphology of $aldh3a1^{-/-}$ larvae in comparison with $aldh3a1^{+/+}$ larvae at 96 hpf. Black scale bar: 500 μm. (E). Adult fish number among different genotypes was in line with *the Mendelian Inheritance* in the first generation of F2: $aldh3a1^{+/+} = 14$, $aldh3a1^{+/-} = 27$ and $aldh3a1^{-/-} = 12$. (F). $Aldh3a1^{-/-}$ zebrafish showed decreased enzyme activity (acetaldehyde as substrate) measured by spectrophotometric analysis in zebrafish lysates at 96 hpf; n = 6 clutches with 46–50 larvae. For statistical analysis Student's t-test was applied, *$p < 0.05$. Bp, base pair. PAM, protospacer-adjacent motif. (For interpretation of the references to colour in this figure legend, the reader is referred to the web version of this article.)

2.5. Aldh3a1 knockout zebrafish larvae exhibited impaired glucose homeostasis and can be further aggravated by endogenous pdx1 expression silencing

Based on the above findings that Aldh3a1 can regulate the morphology and function of the primary pancreas, we hypothesized loss of Aldh3a1 may lead to the imbalance of glucose homeostasis as a consequence of the pancreas dysfunction. A series of metabolomic screenings and glucose determination were performed in *aldh3a1* mutants under normal condition and *pdx1* silencing. The intermediates involved in the citric cycle and pyruvate, the output of glycolysis, showed a declined trend in $aldh3a1^{-/-}$ larvae at 96 hpf (Fig. 7 A–B). Besides, amino acid profile displayed several reduced glycogenic amino acids, including asparagine (Asn), glycine (Gln) and methionine (Met), in $aldh3a1^{-/-}$ zebrafish larvae at 96 hpf (Fig. 7C). Surprisingly, $aldh3a1^{-/-}$ larvae with control morpholino intervention showed the same levels of ATP and ADP compared to $aldh3a1^{+/+}$ larvae with *pdx1* silencing at 96 hpf, while $aldh3a1^{-/-}$ larvae with *pdx1* silencing achieved significantly lowest ATP and ADP level among all groups (Fig. 7D). This result indicated the impaired energy metabolism in *aldh3a1* mutants and got worse in conjunction with hyperglycaemia, which may be the direct reflection of impaired glucose homeostasis. All these metabolomic changes were further confirmed via RNA-Seq GO pathway enrichment analysis, and all core genes showed down-regulated logFC value in the involved seven pathways (Fig. 7E). We also noticed several changes in thiols, sugar level and fatty acids (Fig S5), suggesting a metabolomic function of Aldh3a1 apart from glucose regulation.

Then, around 40% incremental glucose level was determined in $aldh3a1^{-/-}$ larvae at 48 hpf, as a direct indicator of impaired glucose homeostasis; After *pdx1* silencing, glucose levels were increased in both genotypes and $aldh3a1^{-/-}$ gained around 30% more glucose than $aldh3a1^{+/+}$ larvae, implicating the reinforced effect strength (Fig. 7F). Lastly, *aldh3a1* expression was analysed under diabetic condition. Via RT-qPCR based approach, we found a 3-fold increase of *aldh3a1* mRNA among ALDH genes in wild type larvae at 48 hpf after *pdx1* expression silencing (Fig S6). This result further implies Aldh3a1 as an important regulator of glucose homeostasis in diabetes.

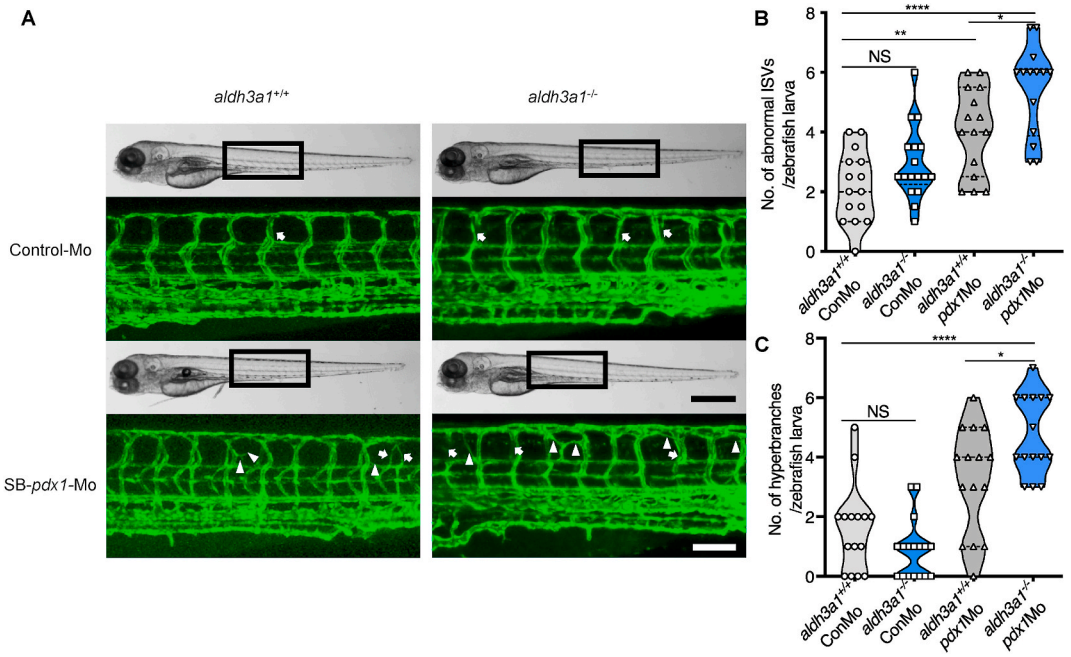

Fig. 3. Trunk vascular alterations were enhanced by endogenous *pdx1* expression silencing in *aldh3a1*$^{-/-}$ *Tg(fli1:EGFP)* zebrafish larvae.
Endogenous *pdx1* expression silencing by *pdx1* morpholino injection led to enhanced formation of abnormal ISVs and hyperbranches in trunk vasculature of *aldh3a1*$^{-/-}$ *Tg(fli1:EGFP)* zebrafish larvae at 96 hpf. (A). Representative light microscopic images showed the gross morphology of zebrafish larvae and black boxes indicate region seen in the confocal images. White arrows indicate the abnormal ISVs and white deltas indicate the hyperbranches. White scale bar = 100 μm, black scale bar = 500 μm. (B–C). Quantification of abnormal ISVs and hyper branches formation in violin plots; n = 15–17 per group. 6 ng of morpholinos: Control-Mo and SB-*pdx1*-Mo were injected into the one-cell stage of zebrafish embryos respectively. For statistical analysis one-way ANOVA followed by Sidak's multiple comparison test was applied, *p < 0.05, **p < 0.01, ****p < 0.0001. *pdx1, pancreatic and duodenal homeobox 1*; ISVs, intersegmental vessels; Mo, morpholino; NS, not significant.

2.6. The elevation of 4-HNE induced the imbalance of glucose homeostasis after Aldh3a1 loss

To test the hypothesis if Aldh3a1 can compensate for the loss of Glo1, as an alternative enzyme for the MG detoxification, while also to identify the responsible factor resulting in the impairment of primary pancreas and glucose homeostasis, we measured corresponding enzyme activities and the concentration of RCS. Unexpectedly, the ability to detoxify MG was changed neither by ALDH nor by Glo1 in *aldh3a1* mutant larvae at 96 hpf (Fig. 8A). Moreover, the MG level was unaltered between wild type and *aldh3a1* mutants, which hints MG is not essential for the vascular phenotype resulting from Aldh3a1 knockout (Fig. 8A). Also, neither glyoxal nor 3-Deoxyglucosone (3-DG) was changed regarding the genotype (Fig S7).

Then, we measured ALDH activity by using 4-HNE as substrate and 4-HNE concentration in *aldh3a1* mutants. Loss of Aldh3a1 caused around 30% reduction of 4-HNE dependent ALDH activity and a 70% increase of internal 4-HNE concentration in zebrafish larvae at 96 hpf (Fig. 8B). Besides, 4-HNE facilitates the formation of 1,4-Michael addition adducts primarily with cysteine [41] and around 20% reduction of free cysteine was observed in *aldh3a1*$^{-/-}$ larvae at 96 hpf (Fig. 8C). This suggests more than a physiological amount of cysteine is united with exceeding 4-HNE and leads to the decreased free cysteine level in *aldh3a1* mutants afterwards.

To evaluate if the increased 4-HNE level causes the described phenotype in *aldh3a1*$^{-/-}$ larvae, a series of 4-HNE incubation assays was performed and 10 μM was selected to perform the experiments, as they are effective and zebrafish larvae show normal gross morphology after incubation (Table S1). First, *ins, insb* and *pdx1* expressions were measured. *Ins* and *pdx1* were significantly reduced after 4-HNE treatment (Fig. 8D), which is in line with both *aldh3a1* transient knockdown and permanent knockout. Also, similar to *aldh3a1* mutants, several reduced glycogenic amino acids, including Asn and Met, were detected in wild type larvae at 96 hpf with 4-HNE incubation (Fig. 8E). Then, glucose was 2.5-fold elevated in wild type larvae at 120 hpf after 4-HNE treatment (Fig. 8F). Lastly, 10 μM 4-HNE incubation exhibited a similar trunk vasculature morphology as compared to Aldh3a1 knockout (Fig S8).

2.7. Exogenous 4-HNE disrupted the pancreas, induced hyaloid vascular alterations via hyperglycaemia, and can be rescued by RCS scavenger treatment

Since *pdx1* silencing induced hyperglycaemia in zebrafish larvae (Fig. 7F) and decreased *pdx1* expression was measured after 4-HNE treatment (Fig. 8D), we detected 4-HNE concentration and ALDH dependent 4-HNE detoxification ability in *pdx1* morphants. However, none of them was changed significantly (Fig. 8G), indicating hyperglycaemia cannot regulate 4-HNE amount in this setting and suggests 4-HNE as the upstream compound to inhibit *pdx1* expression, disrupt pancreas and increase glucose.

To further prove the causal relationship between 4-HNE, pancreas disruption, hyperglycaemia and vascular alterations, and to kick out unspecific side effects of 4-HNE, we observed the pancreas morphology and hyaloid vasculature under 4-HNE incubation and checked out if the rescue effect existed via RCS scavenger and anti-hyperglycaemic intervention. L-Carnosine was chosen as an antioxidant and scavenger of RCS, which protects tissue from 4-HNE induced oxidative damage [42]. Besides, PK11195 was selected as an anti-hyperglycaemic drug, which showed strong effects on decreasing glucose level in hyperglycaemic zebrafish larvae [43].

4-HNE treated zebrafish larvae exhibited reduced dimension of the early primary pancreas (Fig. 9 A–C), in accordance with the changes after *aldh3a1* silencing. 1 mM L-Carnosine treatment showed rescued trend in pancreas disruption caused by 10 μM 4-HNE incubation in both *Tg(hb9:GFP)* and *Tg(ins:nfsB-mCherry)* larvae (Fig S9 and S10); 5 mM and 10 mM L-Carnosine can restore the pancreas morphology significantly (Fig. 9 A-C, Fig S9 and S10). However, PK11195 exhibited no

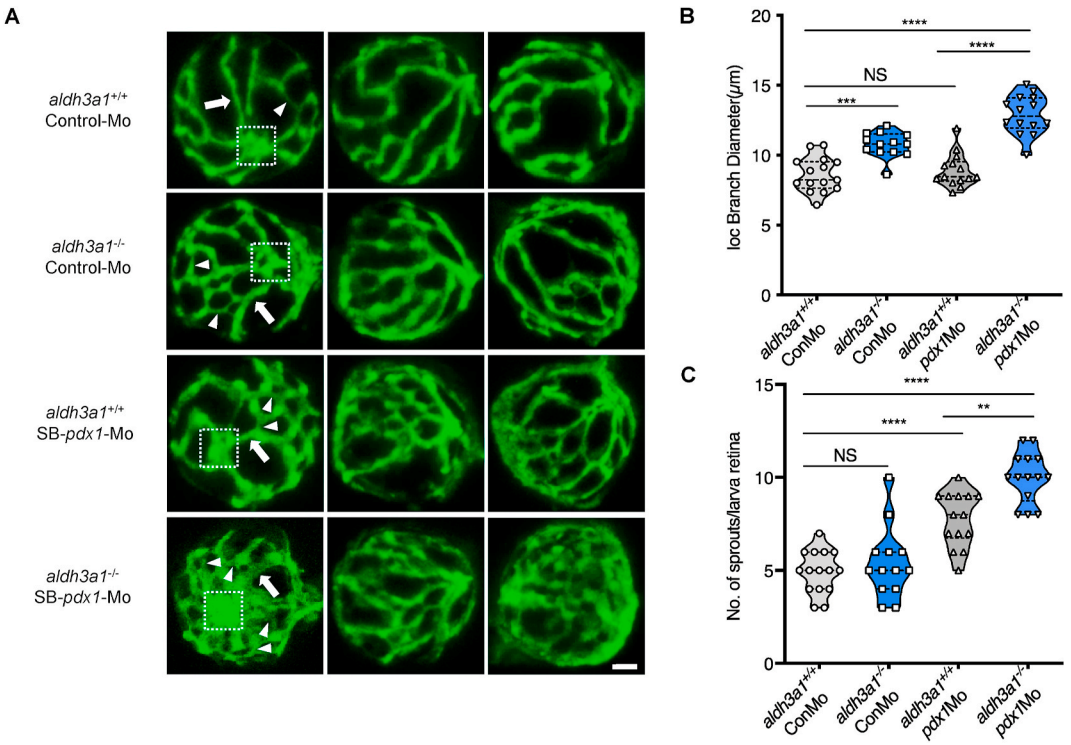

Fig. 4. Retina hyaloid vascular alterations were enhanced by endogenous *pdx1* expression silencing in *aldh3a1*$^{-/-}$ *Tg(fli1:EGFP)* zebrafish larvae. Endogenous *pdx1* expression silencing by *pdx1* morpholino injection led to widening IOC branch diameters and increased sprouts formation in hyaloid vasculature of *aldh3a1*$^{-/-}$ *Tg(fli1:EGFP)* zebrafish larvae at 120 hpf. (A). Representative confocal scans of the isolated hyaloid vasculature in *aldh3a1*$^{+/+}$ and *aldh3a1*$^{-/-}$ larvae after Control-Mo or SB-*pdx1*-Mo injection. At 120 hpf, the hyaloid network has a basket-like structure branching off at the central hyaloid/optic artery (white box) and connects to the circumferential inner annular hyaloid vessel (white arrow) encompassing the lens, also regularly called IOC in the matured adult retinal vasculature. Several sprouts (white delta) interconnect the basket-like vascular arcades and indicate the angiogenesis directly. White scale bar = 20 μm. (B–C). Quantification of the IOC branch diameter and sprouts formation in violin plots, n = 13–15 per group. 6 ng of morpholinos: Control-Mo and SB-*pdx1*-Mo were injected into the one-cell stage of zebrafish embryos, respectively. For statistical analysis one-way ANOVA followed by Sidak's multiple comparison test was applied, **p < 0.01, ***p < 0.001, ****p < 0.0001. Mo, morpholino; IOC, inner optic circle; NS, not significant.

rescue effects on 4-HNE induced pancreas dysfunction (Fig. 9 A–C).

Accompanying with the hyperglycaemia caused by the external 4-HNE intervention (Fig. 8F), we also observed a similar but severe retina hyaloid vascular phenotype compared to *aldh3a1*$^{-/-}$ zebrafish larvae at 120 hpf, with an increase in the branch diameters and significantly elevated vascular interconnection formation, quantified by a higher number of sprouts (Fig. 9D–F). 10 μM PK11195 treatments significantly rescued the angiogenic aspects of sprouts as well as the increased branch diameters in the retina hyaloid network with 10 μM 4-HNE incubation (Fig. 9D–F). Hereby, we identified the angiogenetic retinal hyaloid network is most likely driven by hyperglycaemia after 4-HNE incubation. Furthermore, we illuminate the 4-HNE detoxification is impaired after Aldh3a1 knockout, and the increased 4-HNE concentration acts as the trigger for pancreas disruption, which leads to hyperglycaemia and angiogenetic vascular alterations in the end (Fig. 8G).

2.8. The elevation of serum 4-HNE level in diabetic patients

To assess if the 4-HNE level is also related to the occurrence of diabetes in human beings, 4-HNE measurements in patient sera were performed. Twenty patients from Heidelberg University Hospital were enrolled in the study and were divided into control (n = 9) and type 2 diabetes mellitus (T2DM, n = 11) group according to their disease history. Patient characteristics including age, sex, BMI and biochemical results such as LDL and TG were matched between each group (Table S2). We found that serum 4-HNE level was significantly higher in T2DM patients than in controls (23.19 ± 8.98 *vs*.15.26 ± 5.42 ng/ml, $p = 0.0322$; Fig. 10A). To further investigate the relationship between 4-HNE and development of diabetes, HbA1c and fasting glucose were used as reference parameters for simple linear regression analysis. The accumulation of 4-HNE was found to be significantly positively correlated with both HbA1c ($R^2 = 0.437$, 95% CI of slope 0.047 to 0.168, $p = 0.0015$; Fig. 10B) and fasting glucose level ($R^2 = 0.369$, 95% CI of slope 1.107 to 5.174, $p = 0.0045$; Fig. 10C), suggesting 4-HNE plays a crucial role in the progression of diabetes. Coupled with the finding that 4-HNE interrupts pancreas and causes an imbalance of glucose homeostasis in zebrafish, our clinical evidence further supports the essential function of 4-HNE in diabetes (Fig. 10D).

3. Discussion

In this study, we established an Aldh3a1 knockout zebrafish model for the first time and demonstrated the effects of elevated 4-HNE concentration on glucose homeostasis and the retinal vascular system in zebrafish and the interaction between 4-HNE and diabetes in humans. Elevated endogenous 4-HNE concentration due to Aldh3a1 loss induced impaired glucose homeostasis by the disruption of the primary pancreas, causes a moderate retinal vasodilatory phenotype, and experimental diabetic condition enhances retinal vascular alterations via aggravated glucose homeostasis impairment. Our clinical evidence has further proven the findings, showing the positive correlation between elevated serum 4-HNE and the progression of diabetes.

Diabetes is a group of metabolic disorders characterized by a high blood sugar level over a prolonged time. As the increasing prevalence worldwide, to find out the primary trigger leading to hyperglycaemia in diabetes becomes more and more essential. Unlike type 1 diabetes mellitus (T1DM), the mechanism is clearly described by autoimmune destruction of the β cells and absolute insulin deficiency makes

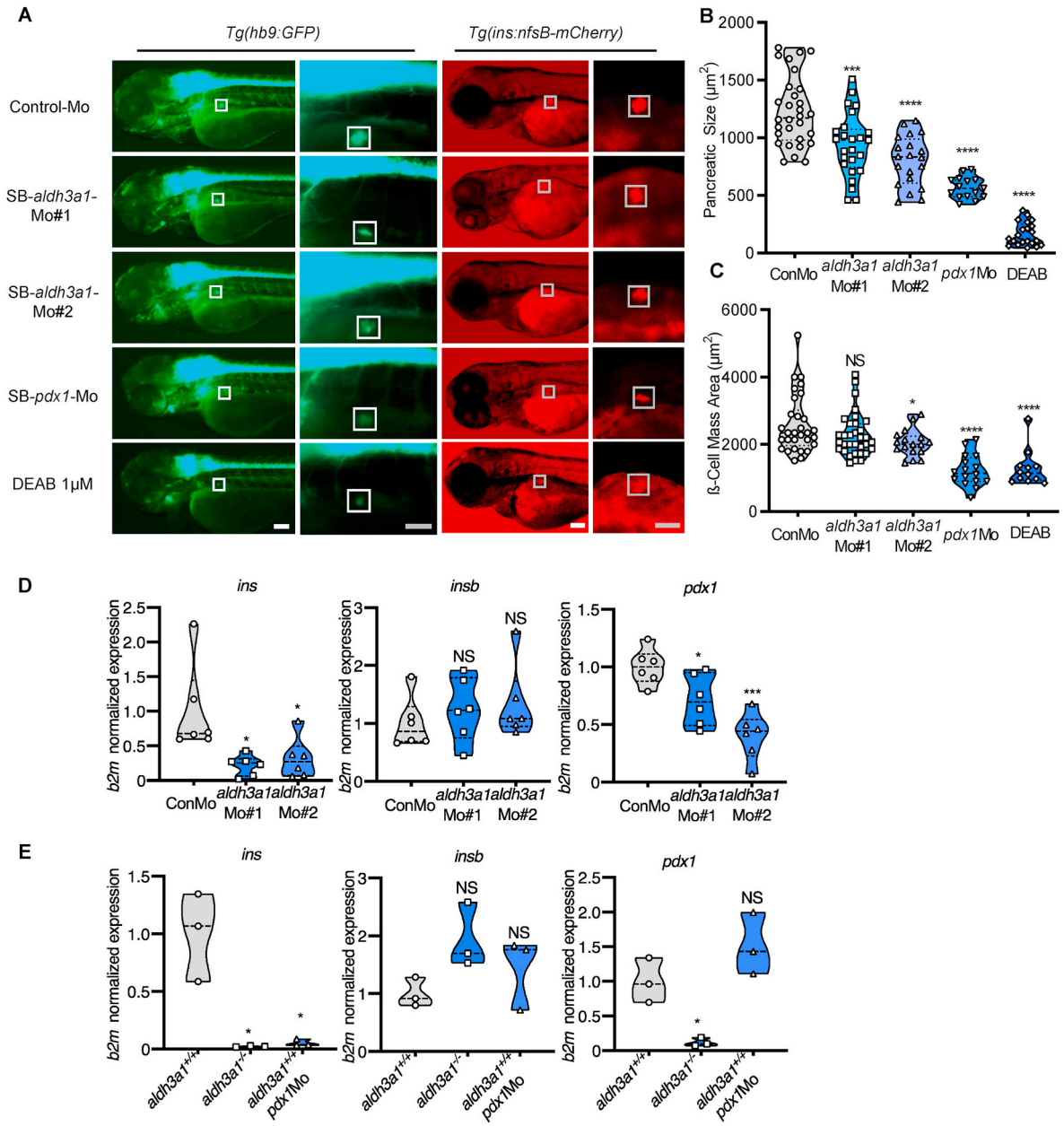

Fig. 5. Primary pancreas was disrupted by ALDH inhibition, *aldh3a1* transient silencing and permanent knockout in zebrafish larvae.
(A). ALDH inhibition by DEAB treatment, and endogenous *aldh3a1* expression silencing induced decreased dimensions of the primary pancreas in *Tg(hb9:GFP)* and a reduced sign of β cell mass area in *Tg(ins:nfsB-mCherry)* zebrafish larvae at 72 hpf. White box indicates the primary pancreas; Grey box indicates the β cell mass area; White scale bar = 100 μm, grey scale bar = 50 μm. (B–C). Quantification of area size of the primary pancreas (B) and β cell mass(C) in violin plots, n = 12–33 per group. (D–E). Similar to *pdx1* morpholino mediated silencing (E), *ins* mRNA expression was decreased significantly in both *aldh3a1* silencing(D) and Aldh3a1 permanent knockout (E) zebrafish larvae at 48 hpf, while *insb* was unaltered. Expression of mRNA was analysed by RT-qPCR and was normalized to *b2m*. The average values of Control-Mo injected (D) and *aldh3a1*$^{+/+}$ zebrafish larvae (E) were standardized to 1, n = 3–6 clutches with 30 larvae per group. 6 ng of each morpholino was injected into the one-cell stage of zebrafish embryos, respectively. For statistical analysis one-way ANOVA followed by Sidak's multiple comparison test was applied, *p < 0.05, ***p < 0.001, ****p < 0.0001. Mo, morpholino; NS, not significant; *ins, preproinsulin; insb, preproinsulin* b; DEAB, N,N-diethylaminobenzaldehyde.

exogenous insulin treatment is required for survival [44], T2DM starts from insulin resistance (IR) of peripheral tissue, linked with reduction of beta-cell mass and compromised insulin secretion ability of beta cells. Behind the IR, several risk-factors may attribute human beings more susceptible to T2DM via the reduction of beta-cell mass, from beta-cell apoptosis to de-differentiation, and precede the onset of T2DM by a decade [45]. However, how these high-risk factors are involved in detail, how they act together and if a "core factor" exists, which promotes insulin resistance to T2DM still requires further exploration. And to understand the mechanisms which "factors" exert their biological effects on the glucose, may help prevent diabetes and define effective therapeutically strategies.

To the best of our knowledge, no research has reported if ALDH3A1 (Aldh3a1) can regulate glucose metabolism yet. Our zebrafish work strongly suggests an increased internal 4-HNE level after Aldh3a1 loss results in hyperglycaemia, providing a novel enzyme linked to diabetes. 4-HNE is often considered as an "escort" when the organism suffers hyperglycaemia. Since high blood glucose liberates non-enzymatic peroxidation of polyunsaturated fatty acids (PUFA) from membrane phospholipids [46], and the peroxidation of PUFA yields bioactive aldehydes, of which 4-HNE is the most prominent [22]. In zebrafish, we identified exceeding 4-HNE due to loss of Aldh3a1 enzyme system

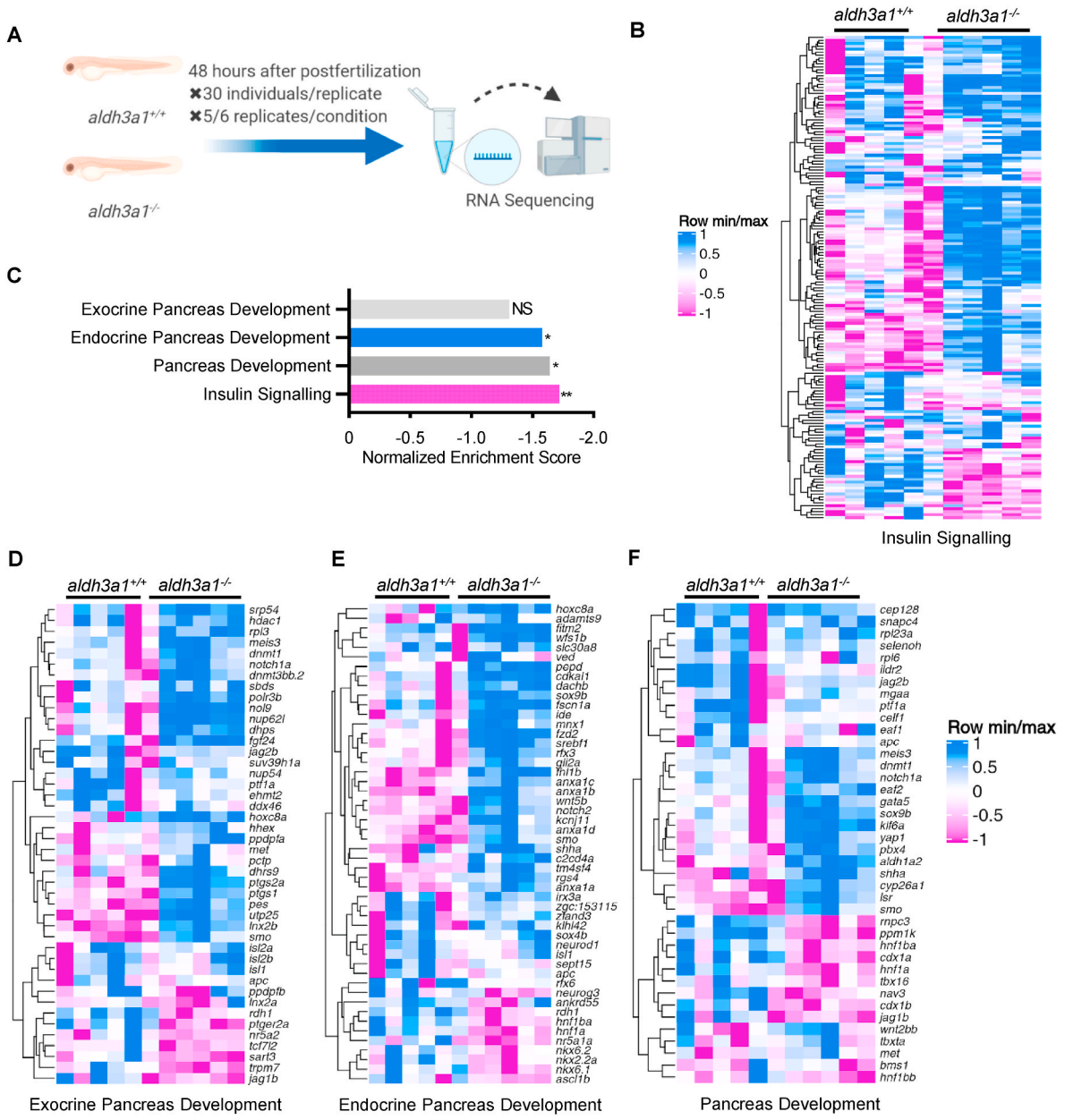

Fig. 6. Down-regulated insulin signalling and endocrine but not exocrine pancreas development pathway in *aldh3a1*$^{-/-}$ zebrafish larvae.
(A). Schematic diagram of larval RNA-Seq. 30 larvae per clutch, 5 clutches of *aldh3a1*$^{+/+}$ and 6 clutches of *aldh3a1*$^{-/-}$ zebrafish larvae at 48 hpf was used for RNA isolation. (B–C). RNA-Seq Heatmap showed relative mRNA expression in insulin signalling pathway (B), which was significantly down-regulated in *aldh3a1*$^{-/-}$ larvae via KEGG analysis (C), **p = 0.003. (D–F). RNA-Seq Heatmap showed relative mRNA expression in exocrine (D), endocrine (E) and whole (F) pancreas development pathway, and endocrine but not exocrine pancreas development pathway was significantly down-regulated in GSEA analysis(C). The higher and lower expression is displayed in pink and blue, respectively. Adjust p value: *p < 0.05, **p < 0.01; NS, not significant; GSEA, gene set enrichment analysis; KEGG, kyoto encyclopedia of genes and genomes.

inhibited the expression of pancreatic development transcription factor Pdx1, disrupted primary pancreas structure and eventually led to impaired glucose homeostasis. This led to the hypothesis, whether 4-HNE is just a marker or the actual maker of hyperglycaemia? To answer the question, a known hypoglycaemic drug PK11195 [43] was used to evaluate if decreasing the glucose level can block the 4-HNE leading effects. 4-HNE caused retina angiogenetic vascular alterations can be rescued by anti-hyperglycaemic therapy; emphasising elevated 4-HNE is the upstream metabolite regulating high blood sugar level. Rather than being a marker for diabetes, this study identified 4-HNE, at least in zebrafish, as a metabolic factor inducing hyperglycaemia.

Consistent with the hyperglycaemia inducer in zebrafish, the elevated 4-HNE level might be a clinical feature in patients with diabetes and diabetic complications [47,48]. Lucia La Sala et al. found that 4-HNE levels were significantly higher in T2DM patients compared to normal glucose tolerance people [49]; Morana Jaganjac et al. observed the progression of T2DM was associated with increased 4-HNE levels in adipocytes [50]. However, the crucial role of 4-HNE in the onset of T2DM requires further investigation. It was shown that increased 4-HNE concentration induced beta-cell apoptosis and impaired insulin secretion in rats [46], which might be a possible mechanism linked 4-HNE with T2DM behind IR. More importantly, as the major end product of lipid peroxidation, 4-HNE is considered to be a bioactive marker of oxidative stress [51], and participates in redox signalling of several stress-associated diseases as “the second messenger of reactive oxygen species” (ROS) [52]. The accumulation of 4-HNE in humans signifies the

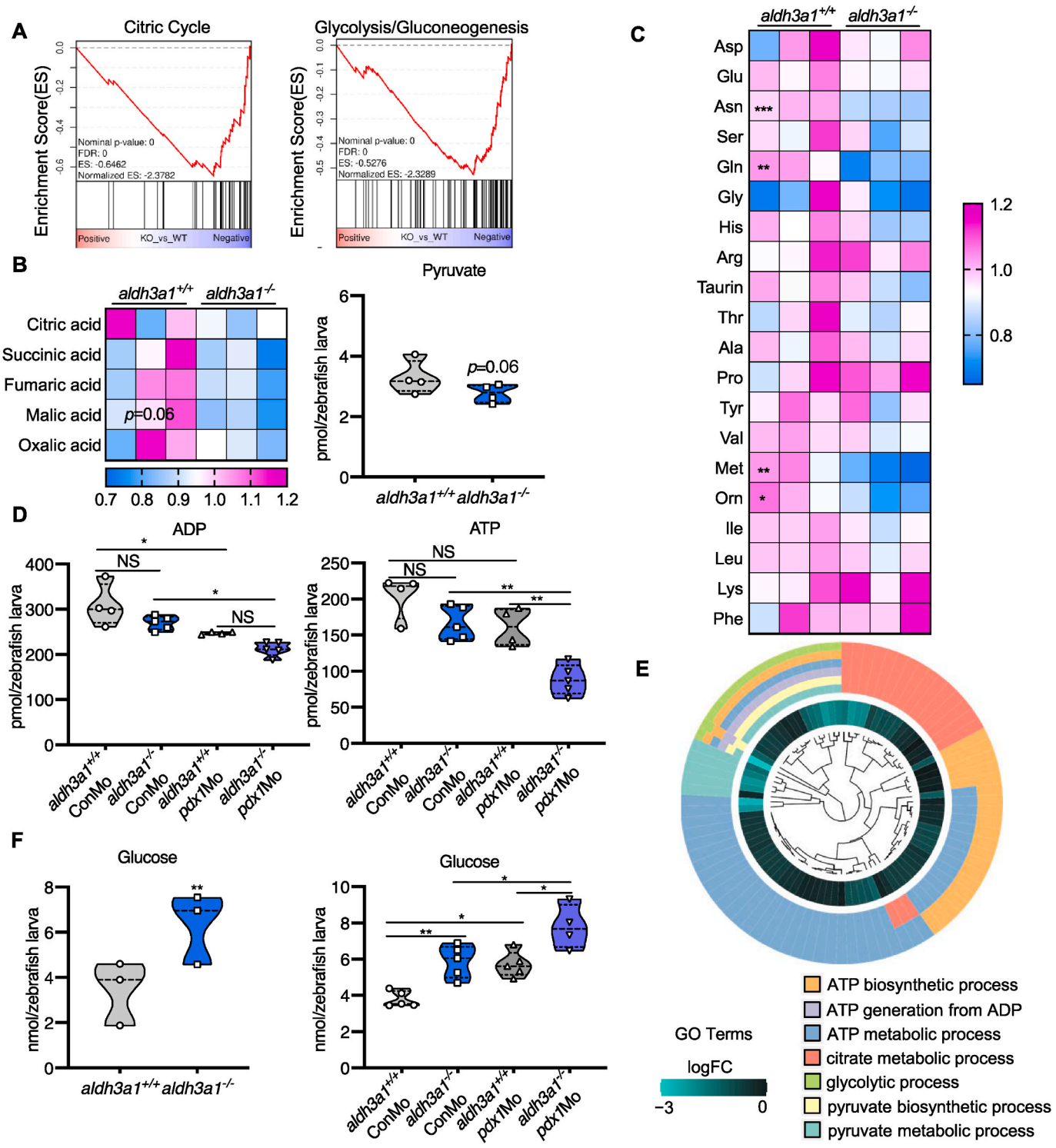

Fig. 7. Aldh3a1 knockout zebrafish larvae exhibited impaired glucose homeostasis and can be further aggravated by endogenous *pdx1* expression silencing.

(A). RNA-Seq GSEA analysis showed down-regulated expression of Citric Cycle and Glycolysis/Gluconeogenesis at 48 hpf; And (B) the intermediates of Citric Cycle and pyruvate showed a decreased trend at 96 hpf in *aldh3a1*$^{-/-}$ zebrafish larvae. (C). Amino acid profile displayed several reduced glycogenic amino acids, including Asn, Gln and Met in *aldh3a1*$^{-/-}$ larvae at 96 hpf. (D) ADP and ATP showed decreased levels in *aldh3a1*$^{-/-}$ larvae and achieved significantly lowest ATP and ADP levels with *pdx1* silencing at 96hpf; (E). All these metabolomic changes were further confirmed via RNA-Seq GO pathway enrichment analysis, and all core genes showed down-regulated logFC value in the involved seven pathways. (F). Increased glucose level was determined in *aldh3a1*$^{-/-}$ larvae at 48 hpf, while *pdx1* silencing enhanced the impaired glucose homeostasis. 6 ng of each morpholino was injected into the one-cell stage of zebrafish embryos respectively. n = 3–6 as each violin plot or heatmap showed. For statistical analysis, paired samples t-tests or one-way ANOVA followed by Sidak's multiple comparison test was applied, *p < 0.05, **p < 0.01, ***p < 0.001. Asn, asparagine; Gln, glycine; Met, methionine.

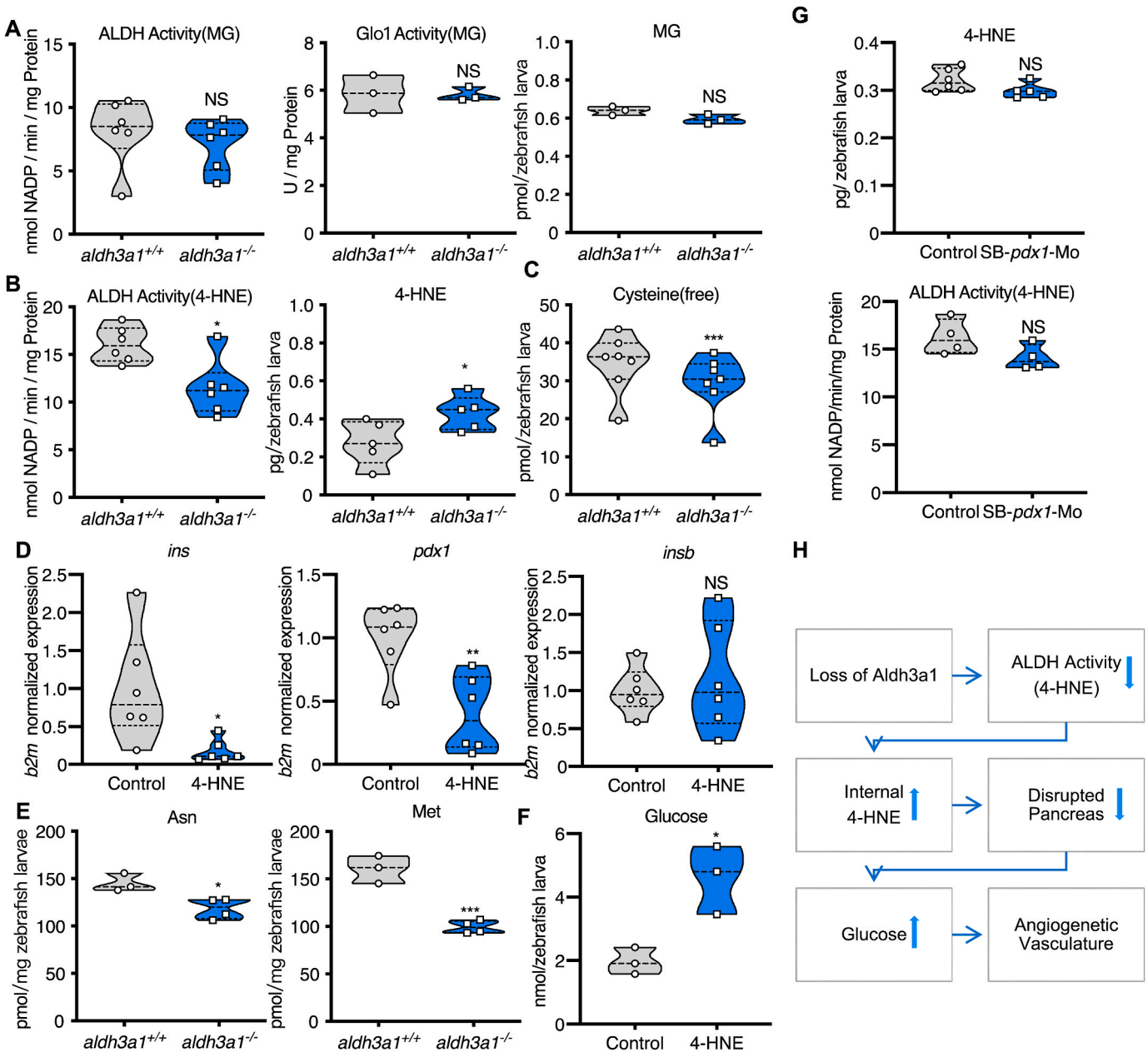

Fig. 8. Defective 4-HNE detoxification and the elevation of 4-HNE induced the imbalance of glucose homeostasis after Aldh3a1 loss.
(A). *Aldh3a1*$^{-/-}$ zebrafish larvae showed unaltered ALDH activity, Glo1 activity when MG as substrate and unchanged MG amount at 96 hpf. (B–C). *Aldh3a1*$^{-/-}$ zebrafish larvae showed decreased ALDH activity when 4-HNE as substrate, increased 4-HNE amount and decreased free cysteine at 96 hpf, but *pdx1* morphants showed no significant change in ALDH activity and 4-HNE amount. (D–F). 10 μM 4-HNE treatment in wild type zebrafish larvae caused: (D). Decreased *ins* and *pdx1* mRNA expression at 48 hpf. Expression of mRNA was analysed by RT-qPCR and was normalized to *b2m*; (E). Reduced glycogenic amino acids Asn and Met at 96hpf; (F). Elevated glucose at 120 hpf. (G). 4-HNE and ALDH dependent 4-HNE detoxification ability were not changed in zebrafish larvae with *pdx1* silencing at 96hpf. (H). Concise mechanism flow chart showed the consequence of defective 4-HNE detoxification after Aldh3a1 loss. n = 3–7 clutches as each plot showed with 30–50 larvae per group. For statistical analysis paired samples t-tests were applied. *p < 0.05, **p < 0.01, ***p < 0.0010.4-HNE, 4-Hydroxynonenal; Glo1, glyoxalase 1; MG, methylglyoxal.

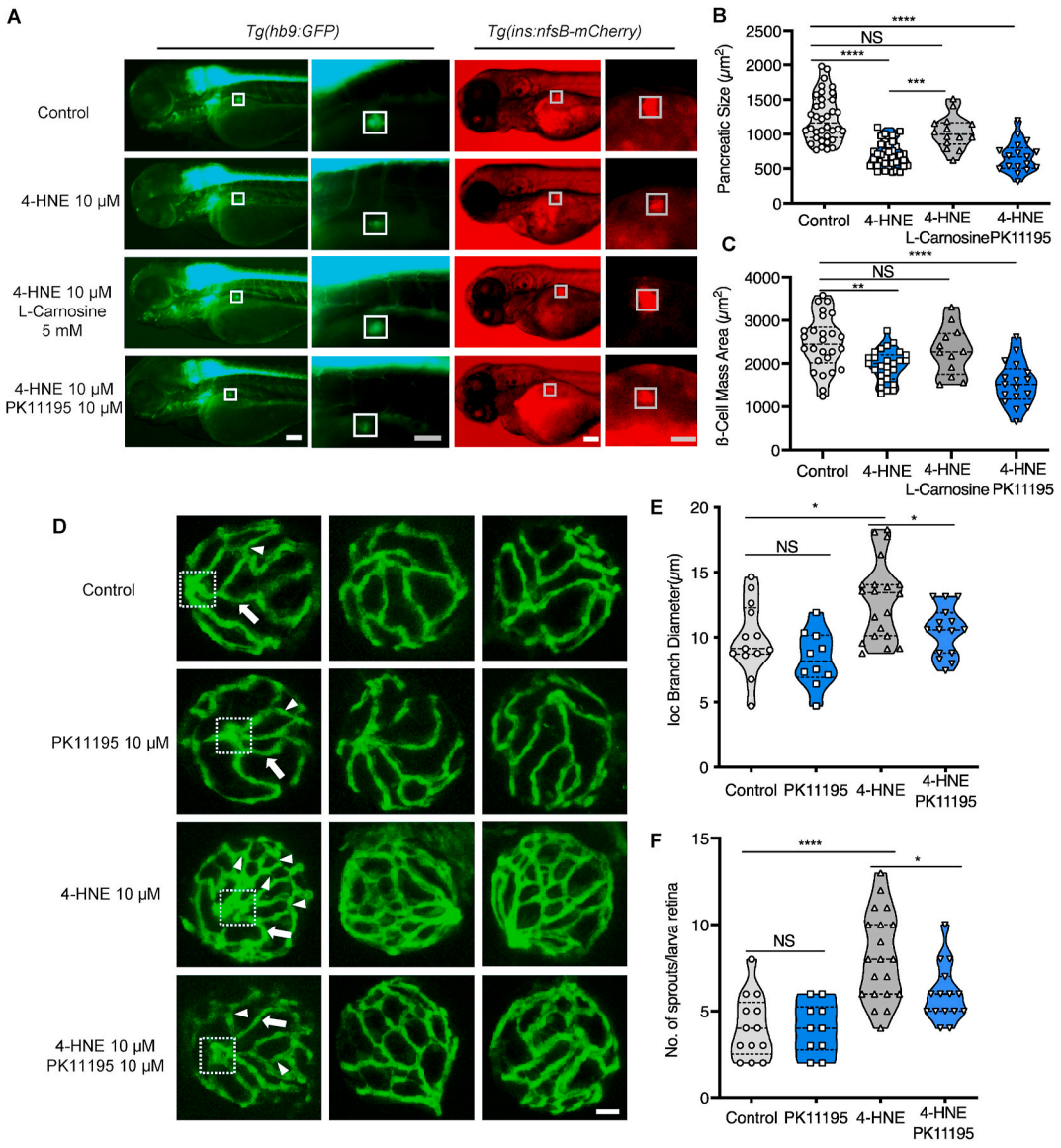

Fig. 9. Exogenous 4-HNE disrupted the pancreas, induced hyaloid vascular alterations, and can be rescued via L-Carnosine and PK11195 treatment, respectively.

(A). 10 μM 4-HNE treatment induced decreased dimensions of the primary pancreas in *Tg(hb9:GFP)* and reduced trend of β cell mass in *Tg(ins:nfsB-mCherry)* zebrafish larvae at 72 hpf, which were rescued by 5 mM Carnosine but not 10 μM PK11195 intervention. Grey box indicates the β cell mass area; White scale bar = 100 μm, grey scale bar = 50 μm. (B–C). Quantification of area size of the early pancreas (B) and β cell mass (C) in violin plots, n = 17–26 per group. (D) 4-HNE incubation led to increased IOC branch diameters (white arrow) and sprouts (white delta) in hyaloid vasculature of *Tg(fli1:EGFP)* zebrafish larvae at 120 hpf, which were rescued via 10 μM PK11195 intervention. White scale bar = 20 μm. (E–F). Quantification of the IOC branch diameters and sprouts in violin plots, n = 10–20 per group. For statistical analysis one-way ANOVA followed by Sidak's multiple comparison test was applied, *$p < 0.05$, **$p < 0.01$, ***$p < 0.001$, ****$p < 0.0001$.

presence of lipid peroxidation and oxidative stress, and for sure, both of which play fundamental roles during the installation and development of T2DM in a certain sense [53].

In addition, within the clinical context, the extent to the correlation between the progression of T2DM and 4-HNE overdose remained unclear. Our clinical finding shows the serum 4-HNE level is correlated with HbA1c and fasting glucose and offers several meaningful implications. First, it suggests human beings share similar 4-HNE detoxification mechanism with zebrafish regarding glucose homeostasis. Using Aldh3a1 knockout zebrafish would be an appropriate disease model for studying the accumulation of blood sugar to diabetic organ damage. Besides, our results suggest new clinical indexes for diabetes assessment: Compare to previous high-risk factors, screening the people with the elevated serum 4-HNE, altered ALDH activity or *ALDH3A1* mutation, and dynamic monitoring the alteration, might be interesting for seeking the people with pre-diabetic state, as well as to prevent diabetes and even the development of complications. Lastly, this work affords a neoteric strategy for diabetes treatment. Traditional therapy relies on hypoglycaemic agents and insulin sensitizer and mostly diabetic patients need to take medications for their whole life to achieve proper glucose control. Whether it would be effective to treat diabetes by using ALDH activity sensitizer, 4-HNE scavenger such as carnosine, and even to cure diabetes and recovery the function of pancreas by eliminating 4-HNE toxic effects, deserves future study.

Notably, even without any high-risk factor, some individuals may be more prone to diabetes due to multiple genetic susceptibilities. Although more than 36 diabetes-associated genes were identified, only about 10% of the heritability of T2DM can be well explained [54]. To the best of our knowledge, no case reported diabetes regarding *ALDH3A1* mutation. Whereas, this study provides a comprehensive transcriptome and

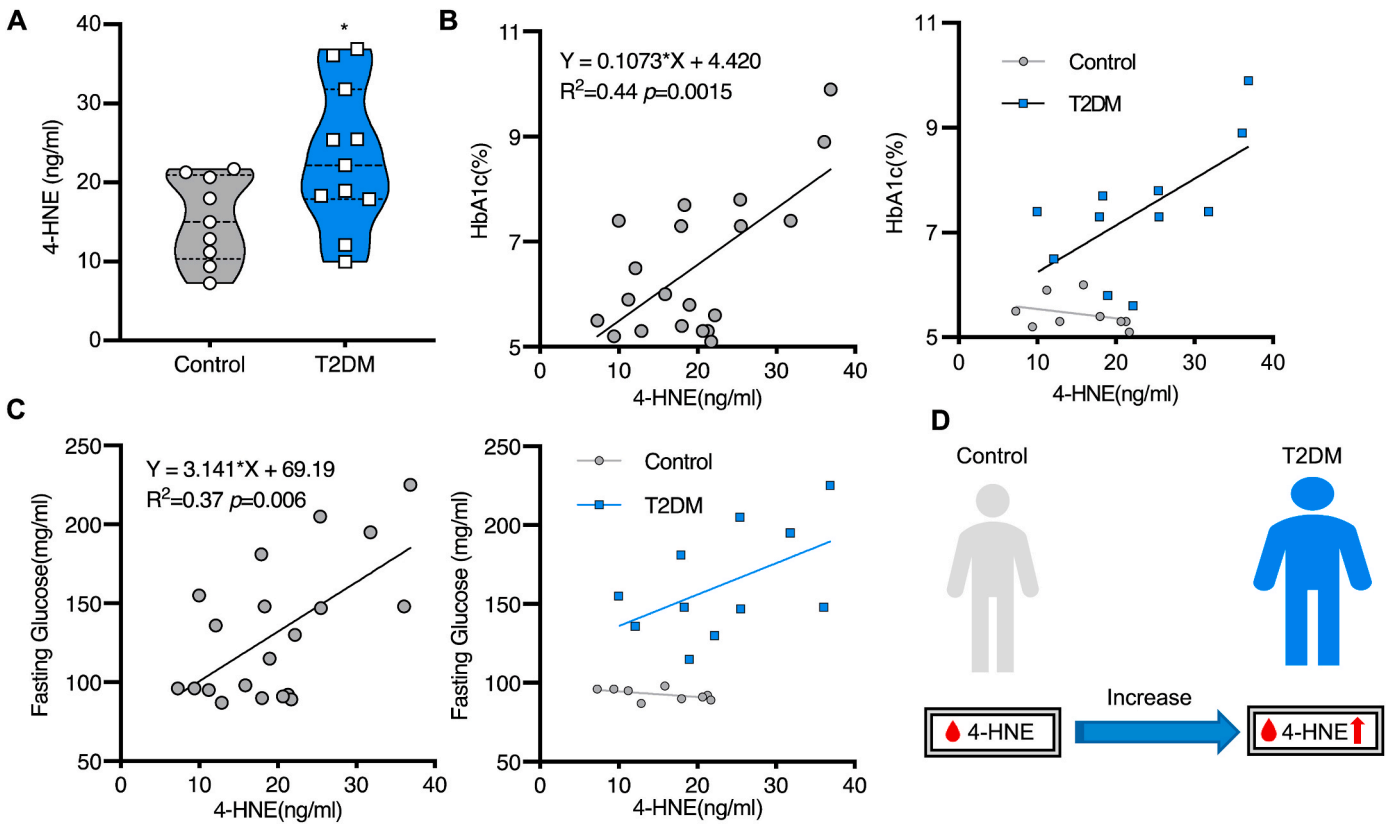

Fig. 10. Increased serum 4-HNE level in T2DM patients.
(A). Serum 4-HNE level was significantly higher in T2DM patients compared to control, for statistical analysis unpaired t-tests was applied, *p = 0.032. (B–C). The simple linear analysis showed 4-HNE was significantly positively correlated with HbA1c (B) and fasting glucose (C). The x-axis represents serum 4-HNE level and the y-axis represents HbA1c (B) and fasting glucose (C) measured by Universitätsklinikum Heidelberg during the patient's hospitalization. 11 T2DM patients and 9 controls were enrolled in the analysis. (D). Increased serum 4-HNE level in T2DM patients.

metabolomic screening regarding how dysfunctional Aldh3a1 impaired glucose homeostasis. Investigating *ALDH3A1* mutation in "susceptible crowd" would be important for diabetes genomic research.

In conclusion, this study provided patent evidence for the contribution of elevated 4-HNE concentration to the development of hyperglycaemia and diabetic retinopathy via pancreas dysfunction in zebrafish *aldh3a1* mutants and the correlation in diabetic patients, as a novel direction for future research regarding early diagnostic screening, pathophysiology and therapy of diabetes.

4. Materials and methods

4.1. Study approval

All patients had been recruited in the study department for diabetes research at the Heidelberg University Hospital and gave written informed consent. Recruitment and tests were part of the Heidelberg Study on Diabetes and Complications (HEIST-DiC), which had been approved by the local ethics committee (ethics number S-383/2016, ClinicalTrials.gov Identifier NCT03022721).

All experimental procedures on animals were approved by the local government authority, Regierungspräsidium Karlsruhe and by Medical Faculty Mannheim (license no: G-98/15, G-160/14 and I-19/02) and carried out in accordance with the approved guidelines.

4.2. Zebrafish husbandry and zebrafish lines

Zebrafish lines, *Tg(fli1:EGFP)* [55], *Tg(hb9:GFP)* (also known as *Tg(mnx1:GFP)* [56] and *Tg(ins:nfsB-mCherry)* [38], were raised and staged as described [57] under standard husbandry environment. Embryos/larvae were kept in E3 media at 28.5 °C with/without PTU (2.5 ml in 25 ml) to suppress pigmentation. Adult zebrafish were kept under 13 h light/11 h dark cycle and fed with living shrimps in the morning and fish flake food in the afternoon.

4.3. Morpholinos

Morpholinos included SB-*pdx1*-Mo, SB-*aldh3a1*-Mo#1, SB-*aldh3a1*-Mo#2 and Control-Mo (GENE TOOLS, LLC; Table S3) were used as recently described [58]. All morpholinos were diluted to 6 μg/μl in 0.1 M KCl. One nanoliter of morpholino was injected into the yolk sack of one-cell stage of the embryos as previously described [68].

4.4. Mutant generation

For mutant generation through the CRISPR/Cas9 technique, one guide RNA (gRNA) targeting exon 2 of *aldh3a1* was designed using the ZiFiT Targeter 4.2 and cloned into a T7-driven promotor expression vector (pT7-gRNA; Addgene) (*Aldh3a1*-CRISPR-for&rev, Table S4). The pT3TS-nCas9n vector (Addgene) was used for in vitro transcription to attain Cas9 mRNA [59]. Synthesis of mRNA for injection was achieved by the use of the mMESSAGE mMACHINE T3 Transcription Kit for Cas9 mRNA and MEGAshortscript T7 Kit for gRNA while following the protocol of the manufacturer (Invitrogen). One nanoliter of 0.1 M KCl solution containing the gRNA (200 pg/nL) and Cas9 mRNA (200 pg/nL) were injected at one-cell stage [59]. F0 mosaic fish were analysed for germline transmission and selectively bred. Genotyping was performed through Sanger sequencing of PCR products (*Aldh3a1*-Genotyping#1.1&1.2) or gel electrophoresis (*Aldh3a1*-Genotyping#1.3&1.4) (Table S4). Mutations were analysed by evaluation of the chromatograms and use of Yost tools [60].

4.5. Microscopy and analysis of pancreatic and vascular alterations in larvae

For in vivo analysis of pancreatic structure, *Tg(hb9:GFP)* and *Tg(ins:nfsB-mCherry)* larvae were anaesthetized in 0.0003% tricaine at 72 hpf. Images were taken with an inverted microscope (Leica DMI 6000 B) with a camera (Leica DFC420C) and the Leica LAS application suite 3.8 and 4.13. The primary pancreas and β cell mass dimension were imaged at 20x and 8x, respectively. Quantification was done by using ImageJ.

For in vivo imaging of the zebrafish trunk vasculature, *Tg(fli1:EGFP)* larvae were anaesthetized in 0.0003% tricaine at 96 hpf, lying on the side. Images were taken via a DM6000 B microscope with Leica TCS SP5 DS scanner with 600 Hz, 1024 × 512 pixels and 1 μm thick z-stacks. For quantification of altered trunk vessels, the first 5 ISVs of each zebrafish larvae were skipped and in the following 17 pairs alterations were counted. The development of new blood vessels referred to 'hyperbranches', and altered intersegment vessels that either miss connections to others (consider as abnormal and count 1 point) or show slight malformations (thin, thick or wrong direction; consider as partially abnormal and count 0.5 point) were grouped as 'abnormal ISVs' and counted.

For in vivo imaging of the zebrafish retinal hyaloid vasculature, *Tg(fli1:EGFP)* larvae were anaesthetized in 0.0003% tricaine at 120 hpf, and fixed in 4% PFA/PBS overnight at 4 °C afterwards. Fixed larvae were washed three times for 20 min in double-distilled water (ddH2O) and incubated for 90 min at 37 °C in 0.5% Trypsin/EDTA solution (25,200–056, Gibco) buffered with 0.1 M TRIS (Nr. 4855.3, Roth) dilution and adjusted to pH 7.8 with 1 M HCl solution. Larval hyaloid vasculature was dissected under a stereoscope and displayed in PBS for visualisation according to Jung's protocol [61]. Confocal images for phenotype evaluation were acquired using a confocal microscope (DM6000 B) with a scanner (Leica TCS SP5 DS) utilising a 20×0.7 objective, 1024× 256 pixels, 0.5 μm Z-steps. IOC branch diameters were measured at two different positions by ImageJ and new blood vessels by neo-angiogenesis were counted and addressed as "sprouts" within the circumference of the hyaloid per sample.

4.6. Pharmacological treatment of zebrafish embryos/larvae

Fertilized zebrafish embryos were transferred into 6-well plate, around 30 embryos per well with 5 ml eggwater. At 24 hpf the chorion of zebrafish embryos was removed using sharp forceps and 0,003% PTU was added to the eggwater. For 4-HNE intervention and rescue experiments, 10 μM 4-HNE (393,204; Sigma-Aldrich), 10 μM PK11195 (C0424; Sigma-Aldrich), 1 mM, 5 mM or 10 mM L-Carnosine (C9625; Sigma-Aldrich) treatments were started at 3 hpf and continued until the end. For ALDH inhibition, 0.25 μM or 1 μM Gossypol (G8761-100MG; Sigma-Aldrich) and DEAB (D86256-100G; Sigma-Aldrich) treatments were started at 3 hpf and continued until the end; Medium was changed every day.

4.7. Whole-body glucose determination in zebrafish larvae

Zebrafish larvae from different developmental time points were collected and snap frozen. Approximately 20–25 larvae per clutch were homogenized in glucose assay buffer with by the ultrasonic homogenizer sonicator, 90% intensity, and 15 s for 2 times. Glucose content was determined according to the manufacturer's instruction (Glucose Assay Kit, CBA086, Sigma-Aldrich).

4.8. 4-HNE determination in zebrafish larvae and patients

Zebrafish larvae from 96 hpf were collected and snap frozen. Approximately 40–50 larvae per clutch were homogenized in PBS by the ultrasonic homogenizer sonicator, 90% intensity, 15 s for 2 times. Patient sera were ready for detection after 1:20 dilution by using sample dilution buffer from the kit.

4-HNE amount was determined according to the manufacturer's instruction (4-Hydroxynonenal ELISA Kit, E4645, Biovision).

4.9. Enzyme activity assay

At 96 hpf, around 50 zebrafish larvae per measurement were anaesthetized with 0.003% tricaine and snap frozen. ALDH activity was assayed at 25 °C in 75 mM Tris-HCl (pH 9.5) containing 10 mM DL-2-amino-1propanol, 0.5 mM NADP and 2 mM MG/4 mM 4-HNE/5 mM Acetaldehyde by measuring the rate of NADP formation at 340 nm [10]. Glo1-activity was determined spectrophotometrically monitoring the change in absorbance at 235 nm caused by the formation of S-D-lactoylglutathione [62].

4.10. MG, 3-DG, and glyoxal measurements

At 96 hpf, around 50 zebrafish larvae per measurement were anaesthetized with 0.003% tricaine and snap frozen. MG, 3-DG, and glyoxal were measured as previously described [12].

4.11. Metabolomic analysis

Detection was done in cooperation with the Metabolomics Core Technology Platform from the Centre of Organismal Studies Heidelberg. At 96 hpf, around 50 zebrafish larvae per measurement were anaesthetized with 0.003% tricaine and snap frozen. Adenosine compounds, thiols, free amino acids, fatty acids and primary metabolites were measured as previously described [12].

4.12. Reverse-transcription quantitative polymerase chain reaction analysis (RT-qPCR)

Total RNA was isolated from *TG(fli1:EGFP)* zebrafish larvae/adult organs at different time points using the RNeasy Mini Kit following the manufacturer's protocol (Qiagen). First-strand cDNA was generated from 1 μg RNA using the Maxima First Strand cDNA Synthesis Kit according to the manufacturer's protocol (Thermo Scientific). Primer design for zebrafish was done using NCBI or by Roche Universal Probe Library Assay Design Centre and primers are listed in Table S5. All samples were used with Power SYBR™ Green PCR Master Mix Kit in 96-well reaction plates. The qPCR reaction was performed with QuantStudio 3 Real-Time-PCR-System.

4.13. RNA-seq analysis

RNA was isolated from *aldh3a1*$^{+/+}$ and *aldh3a1*$^{-/-}$ larvae at 48 hpf. Library construction and sequencing were performed with BGISEQ-500 (Beijing Genomic Institution, www.bgi.com, BGI). Gene expression analysis were conducted by the Core-Lab for microarray analysis, centre for medical research (ZMF). In brief, the main procedure was done with R and Bioconductor using the NGS analysis package systempipeR [63]. Quality control of raw sequencing reads was performed using FastQC (Babraham Bioinformatics). Low-quality reads were removed using trim_galore (version 0.6.4). The resulting reads were aligned to zebrafish genome version danRer11 from UCSC and counted using Kallisto version 0.46.1 [64]. The count data were transformed to log2-counts per million (logCPM) using the voom-function from the limma package [65]. Differential expression analysis was performed using the limma package in R. A false positive rate of $\alpha = 0.05$ with FDR correction was taken as the

level of significance. Volcano plots, chord plot and heatmaps were created using ggplot 2 package (version 2.2.1), GOplot (version 1.0.2) [66] and the complexHeatmap (version 2.0.0) [67].

The RNA-Seq datasets produced in this study are available at GEO (Gene Expression Omnibus, NIH) under the accession number: GSE151770. (https://www.ncbi.nlm.nih.gov/geo/query/acc.cgi?acc=GSE151770).

4.14. Protein sequence alignment

The amino acid sequences of the Aldh3a1 proteins from zebrafish (X1WBM4_DANRE), human (AL3A1_HUMAN) and mouse (AL3A1_MOUSE) were accessed from the UniProt Database (http://www.uniprot.org/). For the comparison, the genes were selected and aligned with the UniProt-own alignment tool (http://www.uniprot.org/align/).

4.15. Software

For zebrafish *aldh3a1* exon/intron region, amino acid and other schematic diagrams generation, websites of Ensembl (https://www.ensembl.org/), Biorender (https://biorender.com/), Smart (http://smart.servier.com/) and Benchling (https://www.benchling.com/) were used. For the quantification of trunk vasculature, primary pancreas and β cell mass area dimension, the Leica LAS V3.8 and V4.13 software was used. Analysis of retinal vasculature was carried out by using LAS AF Lite Software from Leica for taking screenshots, Gimp for image cutting and ImageJ for quantification. The "GCMS solution" software (Shimadzu®) was used for data processing of the GC/MS analysis.

4.16. Statistics

Experimental results are expressed as mean with standard deviation (mean ± SD). Statistical significance between different groups was analysed using Student's t-test or one-way ANOVA (followed either by post hoc Bonferroni's, Sidak's multiple comparison). For clinical results, simple *t*-test was used to compare continuous variables after normality test and χ^2 test was used to compare categorical variables. The simple linear analysis was used to calculate the correlation between HbA1c, fasting glucose and 4-HNE. GraphPad Prism 8.3.0 was used for analyses and *p* values of 0.05 were considered as significant: *p < 0.05, **p < 0.01, ***p < 0.001, ****p < 0.0001.

Author contributions

BL performed experiments, analysed data, and wrote the manuscript. MB and KB performed the analysis of pancreatic and vascular alterations in zebrafish. CS performed RNA-Seq analysis. SK recruited the patients, collected the blood samples. JM and TF performed biochemical experiments and analysed data. RH performed metabolome experiments and analysed data. RH, ZY and PPN gave conceptual and technological advice. JK conceived and designed the study and wrote the manuscript. JK is the guarantor of this work and, as such, has full access to all the data in the study and takes responsibility for the integrity of the data and the accuracy of the data analysis.

For more information

1. Zebrafish Core Facility Mannheim: https://www.umm.uni-heidelberg.de/core-facilities/zebrafish-core-unit/
2. Clinical trials of NCT03022721, Heidelberg Study on Diabetes and Complications (HEIST-DiC): https://clinicaltrials.gov/ct2/show/NCT03022721
3. The RNA-Seq datasets produced in this study are available at https://www.ncbi.nlm.nih.gov/geo/query/acc.cgi?acc=GSE151770.

Declaration of competing interest

The authors declare that no conflict of interest exists.

Acknowledgements

The study was supported by grants from Deutsche Forschungsgemeinschaft (CRC 1118 and IRTG 1874/2 DIAMICOM). The authors acknowledge the support of the China Scholarship Council (CSC 201706280041). The authors thank Dr. Elisabeth Lodd for technical assistance, Björn Hühn for zebrafish maintenance, Dr. Gernot Poschet and Elena Heidenreich for metabolome experiment assistance, Elisabeth Kliemank for patient blood collection assistance, Prof. Dr. Karen Bieback for assistance in RT-qPCR and Dr. Carolina De La Torre for assistance in RNA quality control. The authors thank the Metabolomics Core Technology Platform of the Excellence cluster "CellNetworks" (University of Heidelberg), and the Deutsche Forschungsgemeinschaft (grant ZUK 40/2010–3009262) for support with UPLC-based metabolite quantification. The authors acknowledge the support of the Core Facility Live Cell Imaging Mannheim (DFG INST 91027/10-1FUGG) and the Zebrafish Core Facility Mannheim.

Appendix A. Supplementary data

Supplementary data to this article can be found online at https://doi.org/10.1016/j.redox.2020.101723.

Transparency document

Transparency document related to this article can be found online at https://doi.org/10.1016/j.redox.2020.101723

References

[1] P. Saeedi, I. Petersohn, P. Salpea, et al., Global and regional diabetes prevalence estimates for 2019 and projections for 2030 and 2045: results from the International Diabetes Federation Diabetes Atlas, 9(th) edition, Diabetes Res. Clin. Pract. 157 (2019) 107843, https://doi.org/10.1016/j.diabres.2019.107843 [published Online First: 2019/09/14].

[2] J.M. Forbes, M.E. Cooper, Mechanisms of diabetic complications, Physiol. Rev. 93 (1) (2013) 137–188, https://doi.org/10.1152/physrev.00045.2011 [published Online First: 2013/01/11].

[3] N.G. Congdon, D.S. Friedman, T. Lietman, Important causes of visual impairment in the world today, J. Am. Med. Assoc. 290 (15) (2003) 2057–2060, https://doi.org/10.1001/jama.290.15.2057 [published Online First: 2003/10/16].

[4] E.K. Fenwick, K. Pesudovs, G. Rees, et al., The impact of diabetic retinopathy: understanding the patient's perspective, Br. J. Ophthalmol. 95 (6) (2011) 774–782, https://doi.org/10.1136/bjo.2010.191312.

[5] P.J. Thornalley, Protein and nucleotide damage by glyoxal and methylglyoxal in physiological systems–role in ageing and disease, Drug Metabol. Drug Interact. 23 (1–2) (2008) 125–150, https://doi.org/10.1515/dmdi.2008.23.1-2.125 [published Online First: 2008/06/07].

[6] N. Rabbani, P.J. Thornalley, Glyoxalase 1 modulation in obesity and diabetes, Antioxid Redox Signal 30 (3) (2019) 354–374, https://doi.org/10.1089/ars.2017.7424 [published Online First: 2017/11/22].

[7] P.J. Beisswenger, S.K. Howell, A.D. Touchette, et al., Metformin reduces systemic methylglyoxal levels in type 2 diabetes, Diabetes 48 (1) (1999) 198–202, https://doi.org/10.2337/diabetes.48.1.198 [published Online First: 1999/01/19].

[8] A.K. Berner, O. Brouwers, R. Pringle, et al., Protection against methylglyoxal-derived AGEs by regulation of glyoxalase 1 prevents retinal neuroglial and vasodegenerative pathology, Diabetologia 55 (3) (2012) 845–854, https://doi.org/10.1007/s00125-011-2393-0 [published Online First: 2011/12/07].

[9] T.M. Curtis, R. Hamilton, P.H. Yong, et al., Muller glial dysfunction during diabetic retinopathy in rats is linked to accumulation of advanced glycation end-products and advanced lipoxidation end-products, Diabetologia 54 (3) (2011) 690–698, https://doi.org/10.1007/s00125-010-1971-x [published Online First: 2010/12/01].

[10] D.L. Vander Jagt, L.A. Hunsaker, Methylglyoxal metabolism and diabetic complications: roles of aldose reductase, glyoxalase-I, betaine aldehyde dehydrogenase and 2-oxoaldehyde dehydrogenase, Chem. Biol. Interact. 143–144 (2003) 341–351, https://doi.org/10.1016/s0009-2797(02)00212-0.

[11] S.P. Baba, O.A. Barski, Y. Ahmed, et al., Reductive metabolism of AGE precursors: a metabolic route for preventing AGE accumulation in cardiovascular tissue, Diabetes 58 (11) (2009) 2486–2497, https://doi.org/10.2337/db09-0375 [published Online First: 2009/08/05].

[12] E. Lodd, L.M. Wiggenhauser, J. Morgenstern, et al., The combination of loss of glyoxalase 1 and obesity results in hyperglycemia, JCI Insight 4 (12) (2019), https://doi.org/10.1172/jci.insight.126154.
[13] V. Vasiliou, D.C. Thompson, C. Smith, et al., Aldehyde dehydrogenases: from eye crystallins to metabolic disease and cancer stem cells, Chem. Biol. Interact. 202 (1–3) (2013) 2–10, https://doi.org/10.1016/j.cbi.2012.10.026 [published Online First: 2012/11/20].
[14] R.J. Schaur, W. Siems, N. Bresgen, et al., 4-Hydroxy-nonenal-A bioactive lipid peroxidation product, Biomolecules 5 (4) (2015) 2247–2337, https://doi.org/10.3390/biom5042247 [published Online First: 2015/10/06].
[15] G. Cohen, Y. Riahi, V. Sunda, et al., Signaling properties of 4-hydroxyalkenals formed by lipid peroxidation in diabetes, Free Radic. Biol. Med. 65 (2013) 978–987, https://doi.org/10.1016/j.freeradbiomed.2013.08.163 [published Online First: 2013/08/27].
[16] E. Benedetti, B. D'Angelo, L. Cristiano, et al., Involvement of peroxisome proliferator-activated receptor beta/delta (PPAR beta/delta) in BDNF signaling during aging and in Alzheimer disease: possible role of 4-hydroxynonenal (4-HNE), Cell Cycle 13 (8) (2014) 1335–1344, https://doi.org/10.4161/cc.28295 [published Online First: 2014/03/14].
[17] S. Dalleau, M. Baradat, F. Gueraud, et al., Cell death and diseases related to oxidative stress: 4-hydroxynonenal (HNE) in the balance, Cell Death Differ. 20 (12) (2013) 1615–1630, https://doi.org/10.1038/cdd.2013.138 [published Online First: 2013/10/08].
[18] H. Zhong, H. Yin, Role of lipid peroxidation derived 4-hydroxynonenal (4-HNE) in cancer: focusing on mitochondria, Redox Biol 4 (2015) 193–199, https://doi.org/10.1016/j.redox.2014.12.011 [published Online First: 2015/01/20].
[19] F.J. Pashkow, Oxidative stress and inflammation in heart disease: do antioxidants have a role in treatment and/or prevention? Int. J. Inflamm. 2011 (2011) 514623, https://doi.org/10.4061/2011/514623 [published Online First: 2011/08/24].
[20] K. Okamoto, S. Toyokuni, K. Uchida, et al., Formation of 8-hydroxy-2'-deoxyguanosine and 4-hydroxy-2-nonenal-modified proteins in human renal-cell carcinoma, Int. J. Canc. 58 (6) (1994) 825–829, https://doi.org/10.1002/ijc.2910580613 [published Online First: 1994/09/15].
[21] S. Sasson, 4-Hydroxyalkenal-activated PPARdelta mediates hormetic interactions in diabetes, Biochimie 136 (2017) 85–89, https://doi.org/10.1016/j.biochi.2016.10.007 [published Online First: 2016/10/26].
[22] S. Sasson, Nutrient overload, lipid peroxidation and pancreatic beta cell function, Free Radic. Biol. Med. 111 (2017) 102–109, https://doi.org/10.1016/j.freeradbiomed.2016.09.003 [published Online First: 2016/09/08].
[23] G. Liu, W. Ji, J. Huang, et al., 4-HNE expression in diabetic rat kidneys and the protective effects of probucol, J. Endocrinol. Invest. 39 (8) (2016) 865–873, https://doi.org/10.1007/s40618-015-0428-y [published Online First: 2016/02/03].
[24] E. Akude, E. Zherebitskaya, S.K. Roy Chowdhury, et al., 4-Hydroxy-2-nonenal induces mitochondrial dysfunction and aberrant axonal outgrowth in adult sensory neurons that mimics features of diabetic neuropathy, Neurotox. Res. 17 (1) (2010) 28–38, https://doi.org/10.1007/s12640-009-9074-5 [published Online First: 2009/06/27].
[25] A. Mori, T. Takei, K. Sakamoto, et al., 4-Hydroxy-2-nonenal attenuates beta2-adrenoceptor-mediated vasodilation of rat retinal arterioles, Naunyn-Schmiedeberg's Arch. Pharmacol. 388 (5) (2015) 575–582, https://doi.org/10.1007/s00210-015-1099-0 [published Online First: 2015/02/20].
[26] A. Pappa, D. Brown, Y. Koutalos, et al., Human aldehyde dehydrogenase 3A1 inhibits proliferation and promotes survival of human corneal epithelial cells, J. Biol. Chem. 280 (30) (2005) 27998–28006, https://doi.org/10.1074/jbc.M503698200 [published Online First: 2005/05/21].
[27] S.A. Marchitti, C. Brocker, D. Stagos, et al., Non-P450 aldehyde oxidizing enzymes: the aldehyde dehydrogenase superfamily, Expet Opin. Drug Metabol. Toxicol. 4 (6) (2008) 697–720, https://doi.org/10.1517/17425255.4.6.697 [published Online First: 2008/07/10].
[28] G.P. Voulgaridou, I. Tsochantaridis, C. Tolkas, et al., Aldehyde dehydrogenase 3A1 confers oxidative stress resistance accompanied by altered DNA damage response in human corneal epithelial cells, Free Radic. Biol. Med. (2020), https://doi.org/10.1016/j.freeradbiomed.2020.01.183 [published Online First: 2020/02/02].
[29] N. Lassen, J.B. Bateman, T. Estey, et al., Multiple and additive functions of ALDH3A1 and ALDH1A1: cataract phenotype and ocular oxidative damage in Aldh3a1(-/-)/Aldh1a1(-/-) knock-out mice, J. Biol. Chem. 282 (35) (2007) 25668–25676, https://doi.org/10.1074/jbc.M702076200 [published Online First: 2007/06/15].
[30] R.S. Holmes, J. Hempel, Comparative studies of vertebrate aldehyde dehydrogenase 3: sequences, structures, phylogeny and evolution. Evidence for a mammalian origin for the ALDH3A1 gene, Chem. Biol. Interact. 191 (1–3) (2011) 113–121, https://doi.org/10.1016/j.cbi.2011.01.014.
[31] A. Agalou, M. Thrapsianiotis, A. Angelis, et al., Identification of novel melanin Synthesis inhibitors from crataegus pycnoloba using an in vivo zebrafish phenotypic assay, Front. Pharmacol. 9 (2018) 265, https://doi.org/10.3389/fphar.2018.00265.
[32] S. Konermann, M.D. Brigham, A.E. Trevino, et al., Genome-scale transcriptional activation by an engineered CRISPR-Cas9 complex, Nature 517 (7536) (2015) 583–588, https://doi.org/10.1038/nature14136.
[33] O.F. Cook, The mendelian inheritance of mutations, Science 28 (707) (1908) 86–88, https://doi.org/10.1126/science.28.707.86.
[34] K. Jorgens, S.J. Stoll, J. Pohl, et al., High tissue glucose alters intersomitic blood vessels in zebrafish via methylglyoxal targeting the VEGF receptor signaling cascade, Diabetes 64 (1) (2015) 213–225, https://doi.org/10.2337/db14-0352.
[35] D.A. Babu, T.G. Deering, R.G. Mirmira, A feat of metabolic proportions: pdx1 orchestrates islet development and function in the maintenance of glucose homeostasis, Mol. Genet. Metabol. 92 (1–2) (2007) 43–55, https://doi.org/10.1016/j.ymgme.2007.06.008 [published Online First: 2007/07/31].
[36] T. Bek, Diameter changes of retinal vessels in diabetic retinopathy, Curr. Diabetes Rep. 17 (10) (2017) 82, https://doi.org/10.1007/s11892-017-0909-9 [published Online First: 2017/08/10].
[37] R.A. Kimmel, D. Meyer, Molecular regulation of pancreas development in zebrafish, Methods Cell Biol. 100 (2010) 261–280, https://doi.org/10.1016/B978-0-12-384892-5.00010-4.
[38] H. Pisharath, J.M. Rhee, M.A. Swanson, et al., Targeted ablation of beta cells in the embryonic zebrafish pancreas using E. coli nitroreductase, Mech. Dev. 124 (3) (2007) 218–229, https://doi.org/10.1016/j.mod.2006.11.005.
[39] P.V. Roder, B. Wu, Y. Liu, et al., Pancreatic regulation of glucose homeostasis, Exp. Mol. Med. 48 (2016) e219, https://doi.org/10.1038/emm.2016.6 [published Online First: 2016/03/12].
[40] M.R. Papasani, B.D. Robison, R.W. Hardy, et al., Early developmental expression of two insulins in zebrafish (Danio rerio), Physiol. Genom. 27 (1) (2006) 79–85, https://doi.org/10.1152/physiolgenomics.00012.2006 [published Online First: 2006/07/20].
[41] M. Breitzig, C. Bhimineni, R. Lockey, et al., 4-Hydroxy-2-nonenal: a critical target in oxidative stress? Am. J. Physiol. Cell Physiol. 311 (4) (2016) C537–C543, https://doi.org/10.1152/ajpcell.00101.2016 [published Online First: 2016/07/08].
[42] K. Noguchi, T.F.S. Ali, J. Miyoshi, et al., Neuroprotective effects of a novel carnosine-hydrazide derivative on hippocampal CA1 damage after transient cerebral ischemia, Eur. J. Med. Chem. 163 (2019) 207–214, https://doi.org/10.1016/j.ejmech.2018.11.060.
[43] L.M. Wiggenhauser, H. Qi, S.J. Stoll, et al., Activation of retinal angiogenesis in hyperglycemic pdx1 (-/-) zebrafish mutants, Diabetes (2020), https://doi.org/10.2337/db19-0873.
[44] K.M. Simmons, A.W. Michels, Type 1 diabetes: a predictable disease, World J. Diabetes 6 (3) (2015) 380–390, https://doi.org/10.4239/wjd.v6.i3.380 [published Online First: 2015/04/22].
[45] T. Sun, X. Han, Death versus dedifferentiation: the molecular bases of beta cell mass reduction in type 2 diabetes, Semin. Cell Dev. Biol. 103 (2020) 76–82, https://doi.org/10.1016/j.semcdb.2019.12.002.
[46] G. Cohen, Y. Riahi, O. Shamni, et al., Role of lipid peroxidation and PPAR-delta in amplifying glucose-stimulated insulin secretion, Diabetes 60 (11) (2011) 2830–2842, https://doi.org/10.2337/db11-0347.
[47] L.Q. Li, M.Y. Yao, J.X. Ma, et al., Continuous subcutaneous insulin infusion combined with liraglutide reduced glycemic variability and oxidative stress in type 2 diabetes mellitus: a study based on the flash glucose monitoring system, Endocr. J. 66 (10) (2019) 871–880, https://doi.org/10.1507/endocrj.EJ19-0016 [published Online First: 2019/06/28].
[48] Y. Oruc, F. Celik, G. Ozgur, et al., Altered blood and aqueous humor levels of asprosin, 4-hydroxynonenal, and 8-hydroxy-deoxyguanosine in patients with diabetes mellitus and cataract with and without diabetic retinopathy, Retina (2020), https://doi.org/10.1097/IAE.0000000000002776 [published Online First: 2020/02/25].
[49] L. La Sala, S. Mrakic-Sposta, E. Tagliabue, et al., Circulating microRNA-21 is an early predictor of ROS-mediated damage in subjects with high risk of developing diabetes and in drug-naive T2D, Cardiovasc. Diabetol. 18 (1) (2019) 18, https://doi.org/10.1186/s12933-019-0824-2 [published Online First: 2019/02/26].
[50] M. Jaganjac, S. Almuraikhy, F. Al-Khelaifi, et al., Combined metformin and insulin treatment reverses metabolically impaired omental adipogenesis and accumulation of 4-hydroxynonenal in obese diabetic patients, Redox Biol 12 (2017) 483–490, https://doi.org/10.1016/j.redox.2017.03.012 [published Online First: 2017/03/24].
[51] T. Xu, S. Liu, T. Ma, et al., Aldehyde dehydrogenase 2 protects against oxidative stress associated with pulmonary arterial hypertension, Redox Biol 11 (2017) 286–296, https://doi.org/10.1016/j.redox.2016.12.019 [published Online First: 2016/12/29].
[52] M. Jaganjac, L. Milkovic, A. Gegotek, et al., The relevance of pathophysiological alterations in redox signaling of 4-hydroxynonenal for pharmacological therapies of major stress-associated diseases, Free Radic. Biol. Med. 157 (2020) 128–153, https://doi.org/10.1016/j.freeradbiomed.2019.11.023 [published Online First: 2019/11/23].
[53] F. Ito, Y. Sono, T. Ito, Measurement and clinical significance of lipid peroxidation as a biomarker of oxidative stress: oxidative stress in diabetes, atherosclerosis, and chronic inflammation, Antioxidants 8 (3) (2019), https://doi.org/10.3390/antiox8030072 [published Online First: 2019/04/03].
[54] C. Herder, M. Roden, Genetics of type 2 diabetes: pathophysiologic and clinical relevance, Eur. J. Clin. Invest. 41 (6) (2011) 679–692, https://doi.org/10.1111/j.1365-2362.2010.02454.x [published Online First: 2011/01/05].
[55] N.D. Lawson, B.M. Weinstein, In vivo imaging of embryonic vascular development using transgenic zebrafish, Dev. Biol. 248 (2) (2002) 307–318, https://doi.org/10.1006/dbio.2002.0711.
[56] H. Flanagan-Steet, M.A. Fox, D. Meyer, et al., Neuromuscular synapses can form in vivo by incorporation of initially aneural postsynaptic specializations, Development 132 (20) (2005) 4471–4481, https://doi.org/10.1242/dev.02044.
[57] C.B. Kimmel, W.W. Ballard, S.R. Kimmel, et al., Stages of embryonic development of the zebrafish, Dev. Dynam. 203 (3) (1995) 253–310, https://doi.org/10.1002/aja.1002030302.
[58] A. Jurczyk, N. Roy, R. Bajwa, et al., Dynamic glucoregulation and mammalian-like responses to metabolic and developmental disruption in zebrafish, Gen. Comp.

Endocrinol. 170 (2) (2011) 334–345, https://doi.org/10.1016/j.ygcen.2010.10.010 [published Online First: 2010/10/23].
[59] L.E. Jao, S.R. Wente, W. Chen, Efficient multiplex biallelic zebrafish genome editing using a CRISPR nuclease system, Proc. Natl. Acad. Sci. U. S. A. 110 (34) (2013) 13904–13909, https://doi.org/10.1073/pnas.1308335110 [published Online First: 2013/08/07].
[60] J.T. Hill, B.L. Demarest, B.W. Bisgrove, et al., Poly peak parser: method and software for identification of unknown indels using sanger sequencing of polymerase chain reaction products, Dev. Dynam. 243 (12) (2014) 1632–1636, https://doi.org/10.1002/dvdy.24183 [published Online First: 2014/08/28].
[61] S.H. Jung, Y.S. Kim, Y.R. Lee, et al., High glucose-induced changes in hyaloid-retinal vessels during early ocular development of zebrafish: a short-term animal model of diabetic retinopathy, Br. J. Pharmacol. 173 (1) (2016) 15–26, https://doi.org/10.1111/bph.13279.
[62] A.C. McLellan, P.J. Thornalley, Glyoxalase activity in human red blood cells fractioned by age, Mech. Ageing Dev. 48 (1) (1989) 63–71, https://doi.org/10.1016/0047-6374(89)90026-2.
[63] H.B. Tw, T. Girke, systemPipeR: NGS workflow and report generation environment, BMC Bioinf. 17 (2016) 388, https://doi.org/10.1186/s12859-016-1241-0.
[64] N.L. Bray, H. Pimentel, P. Melsted, et al., Near-optimal probabilistic RNA-seq quantification, Nat. Biotechnol. 34 (5) (2016) 525–527, https://doi.org/10.1038/nbt.3519.
[65] M.E. Ritchie, B. Phipson, D. Wu, et al., Limma powers differential expression analyses for RNA-sequencing and microarray studies, Nucleic Acids Res. 43 (7) (2015) e47, https://doi.org/10.1093/nar/gkv007.
[66] W. Walter, F. Sanchez-Cabo, M. Ricote, GOplot: an R package for visually combining expression data with functional analysis, Bioinformatics 31 (17) (2015) 2912–2914, https://doi.org/10.1093/bioinformatics/btv300.
[67] Z. Gu, R. Eils, M. Schlesner, Complex heatmaps reveal patterns and correlations in multidimensional genomic data, Bioinformatics 32 (18) (2016) 2847–2849, https://doi.org/10.1093/bioinformatics/btw313.
[68] Jianqing She, Zuyi Yuan, Yue Wu, et al., Targeting erythropoietin protects against proteinuria in type 2 diabetic patients and in zebrafish, Molecular Metabolism 8 (2018) 189–202. https://doi.org/10.1016/j.molmet.2017.11.006. https://doi.org/10.1016/j.molmet.2017.11.006.